HHS Public Access

Author manuscript

*Med (N Y)*. Author manuscript; available in PMC 2023 October 14.

Published in final edited form as:

*Med (N Y)*. 2022 October 14; 3(10): 682–704.e8. doi:10.1016/j.medj.2022.07.008.

# Internal checkpoint regulates T cell neoantigen reactivity and susceptibility to PD1 blockade

**Douglas C. Palmer**[1,*,§], **Beau R. Webber**[2,3,4,*,§], **Yogin Patel**[1], **Matthew J. Johnson**[2,3,4], **Christine M. Kariya**[1], **Walker S. Lahr**[2,3,4], **Maria R. Parkhurst**[1], **Jared J Gartner**[1], **Todd D Prickett**[1], **Frank J. Lowery**[1], **Rigel J. Kishton**[1], **Devikala Gurusamy**[1], **Zulmarie Franco**[1], **Suman K. Vodnala**[1], **Miechaleen D. Diers**[2,3,4], **Natalie K. Wolf**[2,3,4], **Nicholas J. Slipek**[2,3,4], **David H. McKenna**[5], **Darin Sumstad**[6], **Lydia Viney**[7], **Tom Henley**[7], **Tilmann Bürckstümmer**[7], **Oliver Baker**[7], **Ying Hu**[8], **Chunhua Yan**[8], **Daoud Meerzaman**[8], **Kartik Padhan**[9], **Winnie Lo**[1], **Parisa Malekzadeh**[1], **Li Jia**[1], **Drew C. Deniger**[1], **Shashank J. Patel**[1], **Paul F. Robbins**[1], **R. Scott McIvor**[1,10], **Modassir Choudhry**[7], **Steven A. Rosenberg**[1,*,§], **Branden S. Moriarity**[2,3,4,*,§], **Nicholas P. Restifo**[1,*,§]

[1]Surgery Branch, National Cancer Institute (NCI), National Institutes of Health, Bethesda, Maryland, USA.

[2]Department of Pediatrics, University of Minnesota, Minneapolis, MN, USA.

[3]Masonic Cancer Center, University of Minnesota, Minneapolis, MN, USA.

[4]Center for Genome Engineering, University of Minnesota, Minneapolis, MN, USA.

[5]Department of Laboratory Medicine and Pathology, University of Minnesota, Minneapolis, Minnesota, USA.

[6]Molecular and Cellular Therapeutics, University of Minnesota, Saint Paul, Minnesota, USA.

[7]Intima Bioscience, Inc. New York, NY, USA.

[8]The Center for Biomedical Informatics and Information Technology (CBIIT), National Institutes of Health, Bethesda, Maryland, USA,

[9]National Institute of Allergy and Infectious Disease (NIAID), National Institutes of Health, Bethesda, Maryland, USA.

[10]Department of Genetics, Cell Biology and Development, University of Minnesota, MN, USA.

[§]Co-corresponding Authors: Douglas Palmer, palmerdc33@gmail.com; Beau R Webber, webb0178@umn.edu; Steven A. Rosenberg, sar@nih.gov; Branden S. Moriarity, mori0164@umn.edu; Nicholas P. Restifo, restifon@mail.nih.gov.
Lead Contact: Douglas Palmer

Contributions

D.C.P., B.R.W., S.A.R., B.S.M. and N.P.R. were involved in study design and had complete access to the data. M.C., S.A.R., B.S.M., P.F.R., R.S.M. contributed to study concepts. B.R.W., D.S., D.H.M., N.J.S., M.D.D. were responsible for manufacturing and validating therapeutic cells. D.C.P., B.R.W., Y.P., C.M.K., F.J.L., R.J.K., D.G., Z.F., S.K.V., K.P., P.M., D.C.D., S.J.P., D.S., N.J.S., M.D.D., M.J.J., W.S.L., N.K.W., L.V., T.H., T.B., O.B. were involved in data acquisition. J.J.G., T.D.P. were involved in quality control of data and algorithms. Y.H., C.Y., D. M., L.J. were involved in data analysis and interpretation. D.C.P., B.R.W, Y.H., L.J. contributed to statistical analysis. D.C.P. and B.R.W. wrote the manuscript. All authors approved the article for submission and publication.

[*]These authors contributed equally.

## Summary

**Background—**Adoptive transfer of tumor infiltrating lymphocytes (TIL) fails to consistently elicit tumor rejection. Manipulation of intrinsic factors that inhibit T cell effector function and neoantigen recognition may therefore improve TIL therapy outcomes. We previously identified the Cytokine-induced SH2 protein (CISH) as a key regulator of T cell functional avidity in mice. Here, we investigate the mechanistic role of CISH in regulating human T cell effector function in solid tumors and demonstrate that CRISPR/Cas9 disruption of CISH enhances TIL neoantigen recognition and response to checkpoint blockade.

**Methods—**Single-cell gene expression profiling was used to identify a negative correlation between high CISH expression and TIL activation in patient-derived TIL. A GMP-compliant CRISPR/Cas9 gene editing process was developed to assess the impact of *CISH* disruption on the molecular and functional phenotype of human peripheral blood T cells and TIL. Tumor-specific T cells with disrupted Cish function were adoptively transferred into tumor-bearing mice and evaluated for efficacy with or without checkpoint blockade.

**Findings—**CISH expression was associated with T cell dysfunction. CISH deletion using CRISPR/Cas9 resulted in hyperactivation and improved functional avidity against tumor derived neoantigens without perturbing T cell maturation. Cish knockout resulted in increased susceptibility to checkpoint blockade *in vivo*.

**Conclusions—**CISH negatively regulates human T cell effector function, and its genetic disruption offers a novel avenue to improve the therapeutic efficacy of adoptive TIL therapy.


## Graphical Abstract

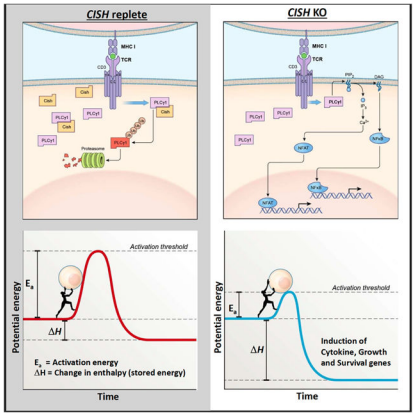


## eTOC Blurb

Genetic engineering of T cells has the potential to improve their efficacy in destroying tumor cells. Palmer et al. demonstrate that knockout of CISH results in improved T cell activation and function, and when combined with PD1 blockade, promotes tumor regression and survival in a preclinical *in vivo* model.

**Keywords**

CRISPR; Checkpoint; scRNAseq; Neoantigen; TIL; PD-1; Immunotherapy; T Cell Therapy; Cancer; CISH

T cells play a prominent role in immune-mediated cancer clearance by targeting tumor cells for destruction through recognition by their T cell receptors (TCRs).[1] Antigen selection is critical, with on-target, off-tumor cytotoxicity resulting in detrimental autoimmunity. Antigens created by somatic mutation—referred to as neoantigens—are appealing as they are expressed specifically by tumor and not somatic tissues. In addition, clinical responses have been associated with higher mutational load in the tumor, attributed to increased frequency of mutation reactive of T cells.[2–6] Neoantigen targeting has been facilitated by next-generation sequencing technologies that allow rapid identification of cognate non-synonymous point mutations in the genome of individual patient tumors.[7] Candidate neoantigens are subsequently loaded onto MHC of autologous antigen presenting cells (APCs) via tandem minigene (TMG) or synthetic peptide pools and used to screen TIL populations derived from resected tumor fragments[8] or PBL.[9] Neoantigen-specific TIL identified in this manner have been attributed to objective clinical responses in a subset of patients with advanced epithelial cancers,[10,11] however achieving consistent clinical success remains a challenge.

The tumor microenvironment and defects in T cell signaling have been attributed to curtailed immune responses to cancer.[12] Substantial effort has been devoted to identifying and understanding factors associated with immune suppression and to devise strategies to overcome them. Markers of T cell activation and exhaustion like PD1, CD39 and TOX have been associated with curtailed immunity to cancer. Recognizing these fundamental limitations prompted us and others[13] to evaluate intrinsic factors that directly inhibit T cell recognition and destruction of tumor cells. We found that CISH (Cytokine-induced SH2 protein), an inhibitor of T cell receptor signaling and tumor immunity in mice,[14] was inversely expressed with these markers of activation/exhaustion. While CISH dysfunction has been associated with susceptibility to multiple chronic infections in humans[15] its role in human immunity against cancer remains is unclear.

Here, we developed a clinical scale, cGMP-compliant manufacturing process for highly efficient and precise CRISPR/Cas9 *CISH* KO in human T cells and TIL. Using this process, we demonstrate that *CISH* KO in neoantigen selected TIL enhances cytokine polyfunctionality, cytolysis and reactivity against identified neoantigens. We also demonstrate that CISH KO unmasks functional reactivity to common *TP53* neoantigens. Furthermore, we show that *CISH KO* enhances the proliferation but not maturation of TIL, and that CISH deletion unleashes an activation and metabolic program that results in the up regulation of multiple activation markers including PD1. Combination therapy of Cish KO TIL generated using our editing process and PD1 blockade resulted in pronounced synergistic cures in a preclinical mouse tumor model. Taken together, these findings demonstrate how loss of internal checkpoints work synergistically with external checkpoint blockade to increase TIL sensitivity to tumor neoantigens. The clinical scale,

cGMP-compliant manufacturing process we have developed for CISH KO in patient-derived TIL offers a near-term opportunity for clinical translation.

## Results

### CISH expression and inducibility in effector T cells

To explore the pattern of *CISH* expression in human TIL, we performed scRNAseq using T cell-enriched fresh TIL obtained from 7 treatment-naive melanoma patients. Combining all samples, t-SNE visualization of the selected gene expression profiles revealed *CD3* gene expression was consistent throughout (Figure 1A). By comparison, CISH exhibited a segregated pattern of expression that was notably distinct from other SOCS family members, a finding we suspected may be due to the unique role of CISH in regulating T cell activation (Figure S1).[16] To explore this further, we next explored the relationship between *CISH* and other known markers of activation. By visual analysis, it appeared that activation markers such as *IFNG*, *PDCD1* (PD1), *TNFRSF9* (41BB), and *HAVCR2* (TIM3) were concomitantly enriched in a pattern inverse to that of *CISH* (Figure 1A). We note that PD1 and TIM-3 can serve as activation or exhaustion markers depending on context, here we are considering these as activation markers due to their inclusion in a broader activation profile. We next segregated T cells into *CISH*-high (above 50% median) and *CISH*-low (below 50% median) and evaluated the expression of other activation markers within these groups. *CISH*-high T cells expressed significantly lower levels of *IFNG, PDCD1, TNFRSF9 and HAVCR2,* while *CISH*-low T cells expressed high levels of these activation/exhaustion markers (Figure 1B), a trend that was consistent across all 7 tumors when analyzed on an individual patient basis (Figure S2). There was however a degree of overlap and we sought to better understand the relationship between CISH and other markers of activation/exhaustion. In subsequent analysis using a cluster-based method computing the gene expression correlation,[17] consistent with previous reports[18–20] we observed a significant positive correlation between PD1 with activation/exhaustion markers TOX[21] and CD39 (ENTPD1) and a negative correlation with the memory marker TCF7[22](Figure 1C). In contrast, CISH expression was negatively associated with TOX and CD39. While there was no significant correlation between CISH and TCF7 expression, we did observe a strong negative relationship between CISH and PD1 mRNA expression.

To evaluate if protein expression would concur with these findings, fresh tumor fragments were obtained from three donors with matched pre-treatment PBL and evaluated for the expression of CISH with PD1 and 41BB. T cells derived from PBL had low levels of 41BB, PD1 and CISH. Consistent with our scRNAseq data and previously published reports,[23] we observed that TIL derived from fresh tumors concurrently express 41BB and PD1 (Figure 1D). In concert with the scRNAseq data, the pattern of *CISH* and *PD1* expression appeared to be mutually exclusive. This differential expression pattern was also observed for CISH and 41BB. To quantify the frequency of CISH expression in TIL, minimally processed tumor resections and patient-matched pretreatment PBL were evaluated for $CD8^+$ T cells and intracellular CISH expression. We observed $CD8^+$ T cells from PBL had low CISH staining regardless of CD45RO status (Figure 1E). In contrast to PBL-derived $CD8^+$ T cells, we found a significant enrichment of CISH expressing $CD8^+$ T cells in TIL directly

from multiple cancer patients (Figure 1F). The lack of CISH expression in CD45RO$^-$ or CD45RO$^+$ PBL derived T cells prompted us evaluate CISH expression and inducibility in different CD8$^+$ T cells subsets. Prior to TCR stimulation, presorted Naïve ($T_N$), Central Memory ($T_{CM}$) and Effector Memory ($T_{EM}$) expressed low levels of CISH. Upon TCR stimulation a significant increase in CISH protein levels was observed, with maximal CISH levels increasing with T cell differentiation status (Figure 1G). TIL are exposed to chronic antigen stimulation and typically skew toward $T_{CM}$ and $T_{EM}$ subsets which may account for the increased expression of CISH in CD8$^+$ TIL. These data indicate in unmanipulated TIL, CISH appears to be inversely expressed with markers of activation and that CISH is not expressed in resting T cells from PBL but is readily induced by T cell activation in a manner that is linked to differentiation status. We sought to further investigate the functional significance of *CISH* in human TIL.

## Feasibility and functionality of CISH deletion in human T cells

To evaluate *CISH* function in human TIL we developed a CRISPR/Cas9-based strategy to knockout *CISH* in human T cells using chemically modified gRNA.[24] To disrupt *CISH* function, we designed and tested a panel of gRNAs targeting two exons shared among *CISH* isoforms and evaluated their activity in primary human T cells (Figure S3A–C).[25,26] Western blot analysis of select highly active gRNAs and one poorly active gRNA confirmed a strong correlation between genetic editing and CISH protein loss relative to controls (Figure S3D). Following TCR stimulation using a CD3-specific antibody, we observed increased IFN-γ production only in cells edited with highly functional gRNAs, confirming that *CISH* KO specifically enhanced functional activation after TCR stimulation (Figure S3E). Based on common targeting of alternate *CISH* splice isoforms and *in silico* analysis of predicted off target activity we selected a specific *CISH* gRNA targeting exon 3 for further evaluation. To characterize the immunological consequences of *CISH* KO, we manufactured *CISH* KO PBL T cells from three healthy donors, achieving an average reduction of CISH protein levels of ~80% (Figure 2A). No alteration in CISH protein expression was observed when targeting the intronic safe harbor locus *AAVS1,* confirming that *CISH* disruption was specific. Following antibody-based CD3 crosslinking, *CISH* KO T cells showed increased IFN-γ, and to a greater degree TNF-α and IL-2 production, resulting in significantly more polyfunctional T cells (Figure 2B). We next evaluated the role of *CISH* KO in an antigen specific response. *CISH* KO T cells were engineered with an HLA-A2 restricted NY-ESO-1-specific TCR and evaluated for cytokine production upon coculture with NY-ESO-1 positive (TC624) and negative (TC526) tumor lines. Whereas only 8% of control T cells were IFN-γ$^+$ TNF-α$^+$ after co-culture, 45% of *CISH* KO T cells were IFN-γ$^+$ TNF-α$^+$ (Figure 2C). Importantly, after CISH KO there was no increase in reactivity against NY-ESO-1 negative targets, We next explored whether the increased polyfunctionality of *CISH* KO T cells enhanced tumor killing. Using a real-time tumor killing assay in relevant (TC624) and irrelevant (TC526) tumor lines, we observed a significant increase in Caspase3 activity in antigen-relevant tumor lines in the presence of *CISH* KO T cells (Figure 2D). *CISH* KO did not alter response to antigen irrelevant tumors, confirming that the effect of the *CISH* KO is restricted to antigen specific recognition via TCR signaling.

### CISH knockout enhances neoantigen reactivity in TIL

The adoptive transfer of neoantigen specific T cells in patients with metastatic cancer can result in profound clinical responses.[10,11] However, identifying neoantigen reactive TIL is difficult and even when reactive TIL are identified, they often have weak reactivities that are lost after *ex vivo* expansion. The difficulties in detection, function, and expansion of neoantigen-specific T cells may be due to the tolerogenic state of these fully mature TIL. We hypothesized that *CISH* KO may reverse this tolerogenic state and enhance TIL neoantigen reactivity. Consequently, we sought to establish a translatable process for *CISH KO* in neoantigen specific TIL (Figure 3A). To evaluate the feasibility and safety of *CISH KO* in TIL, we adapted and optimized a CRISPR-based KO strategy specifically for TIL engineering at clinical scale and in compliance with cGMP guidelines (Figure S4A). Rapid expansion protocols (REP) combining anti-CD3 stimulation and allogeneic PBMC co-culture allow robust expansion of TIL.[27] Prior efforts to incorporate nuclease-based editing into the REP carried out electroporation midway through the procedure. This strategy necessitates electroporation of large numbers of TIL (>1e9) and therefore requires large amounts of editing reagent. It also involves the electroporation of a TIL/PBMC co-culture which can reduce the amount of reagent delivered specifically to TIL. As lymphocyte activation enhances nucleic acid delivery and genome editing.[28] we modified the standard REP procedure by incorporating an initial feeder-free activation step using plate-bound anti-CD3 and soluble anti-CD28 prior to electroporation (Figure S4A) Following CRISPR electroporation, the TIL are transferred to PBMC feeder co-culture for REP. Using this approach, *CISH* KO in human TIL averaged >95% efficiency as measured by sequencing and TIDE analysis (Figure S4B).[29] CISH protein loss correlated well with indel frequency at the targeted locus, averaging >95% protein reduction across the three donors (Figure S4C).

Off target (OT) editing is a key concern for production of a cellular therapy.[30,31] To evaluate OT editing, we utilized computational prediction followed by targeted next generation sequencing (NGS). At 43 candidate OT sites, we did not observe editing above the limit of detection (~0.01%) (Table S1). We also employed unbiased identification of double-strand breaks (DSBs) enabled by sequencing (GUIDE-seq) in TIL.[32] This technique has a lower sensitivity per OT site (detecting locus modification at frequencies of approximately 1%), but is not limited to any theoretical assumptions, e.g., based on sequence homology. Using this complementary approach, we detected no OT events with either approach (Figure S4D). Thus, using two independent and complementary assays, we did not detect any OT editing in TIL modified using our *CISH*-targeting CRISPR/Cas9 reagents.

We next monitored homeostatic TIL proliferation and survival *in vitro* following CRISPR editing and REP and found that CISH KO increased TIL survival and proliferation across a dose-titration of IL-2 (Figure S4E). In addition, CISH KO TIL sustained proliferation longer and to a greater degree compared to controls in long-term (21 day) cultures supplemented with high IL-2 (Figure S4F). To rule out the possibility that *CISH* KO confers the capability of cytokine-independent growth, we removed IL-2 and observed a rapid and complete loss of viable TIL in both the *CISH* KO and WT cultures (Figure. S4G). Thus, despite having significantly enhanced proliferative capacity, *CISH* KO TIL remain dependent on cytokine signaling. This phenotype may be explained by the known role of CISH in negative

regulation of cytokine receptor signaling, including IL-2, as we did not observe notable differences in surface expression of IL-2R chains (Figure S5A–C) or altered memory marker expression in CISH KO TIL (Figure S5D–F). Thus, CISH KO may exert a dual benefit in the context of TIL ACT by both increasing TCR functional avidity and enhancing proliferation and survival under conditions of limiting cytokine availability.

Having established a clinically scalable, high-efficiency *CISH* editing process with a robust safety profile, we wanted to evaluate if this manipulation would result in enhanced reactivity against neoantigens. TIL were isolated from resected tumor fragments from three independent patients, and following whole exome and RNA-sequencing, mutation reactive TIL populations were selected as previously described.[7] TIL were isolated from a tumor resection from a 36-year-old female with metastatic colon cancer, referred to as patient A. The selected TIL population was screened against individual peptides and the cognate neoantigen was identified as GTF2E1 (S334F) (Figure S6). The neoantigen reactive TIL fragment was subjected to the approach as described in Figure 3A) and evaluated for *CISH KO* and functionality against GTF2E1 (S334F). Following CRISPR editing and REP, we measured CISH protein by Western blot and observed the near-complete absence of CISH protein in the CRISPR treated TIL (~97% reduction) (Figure 3B). Next, we wanted to determine if *CISH* KO would enhance TIL recognition and functionality against the GTF2E1 (S334F) neoantigen. Autologous DCs were loaded with GTF2E1 peptide and co-cultured with control or *CISH* KO TIL for 6 hours and evaluated for production of effector cytokines. We found a highly significant increase in the percentage of IFN-γ, IL-2, and TNF-α positive $CD3^+$ T cells in the *CISH* KO TIL compared to controls (Figure 3C). No reactivity was observed against the wildtype (WT) GTF2E1 peptide-pulsed DCs by either *CISH* KO or control TIL. Further, maximal reactivity was maintained even at low levels of GTF2E1 neoantigen, indicating that *CISH* deletion not only increases the overall functionality of TIL but also enhances their sensitivity to antigenic stimulation. This later facet may prove critical *in vivo* where many tumors express low levels of peptide loaded MHC. In addition to increased production of individual cytokines, *CISH* KO TIL also exhibited enhanced polyfunctionality (IFN-γ, TNF-α and IL-2 positive) (Figure 3D). IFN-$\gamma^+$TNF-$\alpha^+$ frequency increased from 17% to 51% in CISH KO TIL, and there was a significant increase in IFN-γ, TNF-α, and IL-2 triple positive TIL. The ability to successfully delete CISH in fully mature human TIL and dramatically increase neoantigen sensitivity and polyfunctionality in this patient propagated us to evaluate to reproducibility across patients.

To verify our approach, a tumor from a 44-year-old male with colorectal cancer, patient B, was resected and TILs were outgrown for neoantigen screening. Reactive cultures were selected and QSOX2 (R524W) was identified as the target neoantigen (Figure S7A). Further characterization revealed that reactivity was mediated predominantly by a population of $CD8^+$ TIL bearing the clonotypic $Vb17^+$ TCR (Figure S7B). Since there was a predominant population of neoantigen specific T cells, we sought to determine if there was an increase in the intensity of cytokine production on a cell-by-cell basis. Editing at *CISH* was highly efficient (Figure 3E), and we found a pronounced increase in the frequency and intensity of IFN-γ staining in the *CISH* KO TIL compared to the control TIL against mutant-QSOX2 loaded APCs (Figure 3F). By contrast, WT QSOX2 peptide did not elicit IFN-g release

in either TIL group. Using titrated neoantigen peptides, we found a significant increase in specific intensity of IFN-γ and TNF-α but not IL-2 in *CISH* KO TIL compared to control TIL (Figure 3G). Despite a significant increase in functionality to mutant QSOX2 by *CISH* KO TIL, reactivity to WT QSOX2 was not detectable at any peptide concentration. From these data, it appears that *CISH* KO reproducibly increases the neoantigen-specific reactivity on a cell-by-cell basis as evidenced by a qualitative increase in cytokine production and TIL polyfunctionality, without increasing reactivity to WT antigens.

In some instances, the detection of neoantigen specific TIL in the initial screening is either lost or significantly diminished after a REP.[33] Although the mechanisms underlying this phenomenon are unclear, it could possibly result from a decrease in the clonal frequency of neoantigen reactive TIL and/or diminished functionality of TIL following rapid expansion. As CISH can enhance TIL functionality against neoantigens, we sought to evaluate if the increased functional avidity afforded by *CISH* KO would resurrect detectable functionality in an instance where neoantigen reactivity became undetectable after a REP. To this end, we evaluated TIL from a 45-year-old female with sigmoid colon cancer, patient C, whose TIL ultimately lost neoantigen reactivity after a REP (data not shown). Following whole exome sequencing, candidate peptides were generated and pooled to test reactivity to TIL derived from fragment F9. Subsequent parsing revealed TIL to be specific to the neoantigen ALOX5AP (K153R) (Figure 3H). This neoantigen-reactive TIL population was then subjected to REP with and without *CISH KO* (Figure 3I). Upon co-culture with autologous APCs loaded with titrated concentrations of mutant ALOX5AP peptide, we found that control TIL had no detectable reactivity to mutated ALOX5AP peptide as measured by staining for IFN-γ, IL-2 or TNF-α (Figure 3J). In contrast, we detected neoantigen reactive T cells after *CISH* KO with significant and titratable increases in IFN-γ, IL-2 and TNF-α. Moreover, WT antigen did not elicit a functional response in either group. These data indicate that loss of neoantigen reactivity after traditional TIL REP can be restored by *CISH* KO, resulting in a significant increase in TIL functionality against a tumor neoantigen.

## CISH as a determinant of neoantigen reactivity

*TP53* mutations are frequent in many cancers and can be presented as neoantigens, however only a subset of patients harbor T cells that elicit a functional immune response.[34] As CISH KO enhances and restores neoantigen reactivities in TIL, we sought to evaluate whether CISH may dampen the T cell response to common *TP53* mutations. To this end, we evaluated RNA-seq from fresh resections that contained *TP53* driver mutations and that we had tested for mutant p53 neoantigen reactivity. We evaluated 18 resections identified with TP53 driver mutations: In 7 of these, we found neoantigen reactivity, whereas we were unable to identify reactivity in 11 of these, which we classify as non-reactive. To filter the heterogeneity often found within these tumor resections we applied a commonly used immunologic filter.[35] We observed delineated clustering among the TP53 neoantigen reactive and non-reactive resection fragments (Figure S8A). Volcano plot analysis displays relative gene expression, with cut off being >1.5 $Log_2$ fold change and p value > 0.05 shaded in gray (Figure 4A). Interestingly, the target antigen *TP53* and activation marker PD1 (*PDCD1*) expression were not significantly different in either group. However, we

found genes associated with T cell activation such as *TNF*, *IL6*, *PRDM1*, *IL1B* and chemokines *CCL3* and *CXCR4* upregulated in reactive resections. This was reflected by the enrichment of activation, differentiation, chemoattraction and signaling GSEA profiles in reactive resected fragments (Figure S8B). Conversely, *CISH* was most highly expressed in the non-reactive fragments (Figure 4A) and was not associated with T cell activation genes(Figure 4B). From these data it appears that *CISH* is preferentially expressed in non-reactive tumor resections, while reactive tumor resections exhibit a profile of T cell activation. Uncovering T cell reactivity to shared “hot spot” TP53 mutations would obviate the laborious process of delineating individual neoantigen TCRs for every patient.[36] The KO of CISH may improve their reactivities and make shared antigen targeting more universal. Thus, we sought to evaluate if CISH deletion would uncover reactivities from a patient with a TP53 hotspot mutation and known specificity with tetramer positive T cells.

We obtained a TIL fragment from a 36 year old female patient with metastatic colorectal cancer, patient D, that had modest neoantigen reactivity to p53 (R175H) in the context of HLA-A0201 and for which we had an estimate of precursor frequency based upon tetramer staining.[37] With a known precursor frequency, we could determine if the increase in reactivity after *CISH* KO was due to an enhancement in T cell function or simply an increased abundance of specific T cells. After *CISH* KO by CRISPR, we performed flow cytometry for p53 HLA-A0201 tetramer and evaluated TIL for reactivity to peptide and p53 (R175H) expressing tumor. We found no discernible change in tetramer staining between control and *CISH* KO T cells (~60% of T cells in both groups) (Figure 4C). Intracellular cytokine staining was performed after coculture with antigen loaded APCs (Figure 4D). We found that both the control and *CISH* KO neoantigen specific T cells elicited no functional response against non-mutated p53. In the presence of mutated p53 there was a dramatic increase in IFN-$\gamma$ staining from 5.4% in the control to 40.7% in *CISH* KO, with approximately a log increase in staining intensity. Similarly, there was a dramatic increase, from 5.1% to 32%, in polyfunctional cytokine production of IFN-$\gamma^+$TNF-$\alpha^+$ after *CISH* KO. Interestingly, bypassing TCR signaling using PMA/ION revealed no general functional defects in the control or *CISH* KO T cells. To evaluate T cell immunity to a naturally processed and presented neoantigen, modified T cells were cocultured with HLA-matched tumors ectopically expressing full length WT or mutant p53 for 6 hours and stained for expression of intracellular cytokines (Figure 4E). Like neoantigen peptide loaded APC’s, we saw an increase in cytokine production after *CISH* KO. In addition, no difference between control and *CISH* KO T cells when TCR signaling was bypassed using PMA/Ionomycin, indicating that CISH specifically inhibits TCR signaling in an antigen-specific manner. It is important to note that while there were similar quantities of mutant p53-tetramer positive T cells in both CISH expressing and KO groups (Figure 4C), only 5% of the control T cells were IFN-$\gamma$ positive, and at a low MFI.

Increases in effector cytokine production typically lead to a decrease in expansion and accelerated T cell maturation.[38,39] To determine the influence of *CISH* KO on this process, we disrupted *CISH* in PBL and TIL and measured expansion and phenotype. *CISH* KO PBL and TIL exhibited a slight increase in expansion compared to no electroporation (UTX) or unmanipulated controls (Figure 4F). Phenotypic analysis found that PBL retained a less differentiated CD45RO$^-$CD45RA$^+$ phenotype compared to TIL, and there was a slight

increase in the $CD45RO^{-}CD45RA^{+}$ population in CISH KO PBL T cells (Figure 4G). These results suggest that *CISH KO* may not influence T cell maturation, although further studies are needed to better understand the apparent contradiction in hyper-effector function in the absence of hyper-maturation.

## CISH KO enhances T cell expansion and function but not maturation

PBL is a complex mixture of T cells and may not clearly represent the subtle changes in T cell maturation. Thus, we evaluated a pure population of undifferentiated T cells in which we could follow their maturation. To this end, we enriched naïve $CD8^{+}$ T cells and studied their expansion, metabolism and maturation after stimulation with or without *CISH* KO. Here, we observed a significant increase in expansion 10 days after TCR stimulation and cytokine support of $CD8^{+}$ *CISH* KO T cells compared to control T cells (Figure 5A). CISH deletion has been shown to enhance NK cell metabolism.[40] To evaluate if this was also true in T cells, after expansion T cells from these six donors were subjected to metabolic analysis using Ultra-HPLC-MS/MS with or without TCR stimulation. CISH KO resulted in an increase in many metabolites in glycolysis, TCA cycle and lipid metabolism which was even more pronounced 4 hours after TCR stimulation (Figure S9A). In fully mature TIL, OCR analysis revealed that CISH KO resulted in an increase in both basal and spare respiratory capacity (Figure S9B). After expansion of naive-derived CISH deleted $CD8^{+}$ T cells we evaluated the maturation state using CD62L and CD45RO. Surprisingly, we did not observe a change in gross phenotypic composition in either group (Figure 5B). However, cytokine support in addition to TCR stimulation can enhance T cell maturation and may mask subtle changes. While overall less mature in the absence of cytokine support, there were no overt changes in T cell maturation with or without *CISH* KO (Figure 5B). This observation that *CISH* KO increases T cell functionality, killing, and expansion without influencing maturation is in stark contrast to our current understanding of the progressive maturation model.[38,39] To further probe this observation, we investigated the molecular underpinnings that could account for this divergence.

In mice, we observed that Cish interacts with and facilitates the degradation of the TCR signaling intermediate Phospholipase C-$\gamma$1 (PLC-$\gamma$1).[16,41] We also have previously established that effects of CISH on T cells are independent of its documented effects on IL2 receptor chains such as CD25, CD122, and CD132.[16] Thus, we systematically evaluated the TCR signaling cascade in *CISH* KO human T cells for deviations that might account for this hyper-activation without hyper-maturation paradox. *CISH* KO $CD8^{+}$ naïve-derived human T cells were expanded for 10 days, rested overnight in the absence of cytokine, then stimulated with TCR crosslinking and evaluated by immunoblot for early, intermediate, and late signaling factors.[42,43] TCR signaling factors ZAP70 and LAT are phosphorylated early after TCR ligation,[44] however we did not observe any changes in the phosphorylation kinetics or intensity of ZAP70 or LAT in the presence or absence of *CISH* following TCR stimulation (Figure 5C). Intermediate signaling factors PLC-$\gamma$1 and SLP76 are critical in propagating the TCR signaling cascade that bridges antigen recognition with transcriptional mediators.[44] We detected a strong increase in the intensity and duration of PLC-$\gamma$1 and SLP76 phosphorylation after TCR stimulation in *CISH* KO T cells compared to control T cells (Figure 5D).

Activation of the PLC/SLP76 complex results in the cleavage of phosphatidylinositol 4,5-bisphosphate (PIP2) into inositol 1,4,5-trisphosphate (IP3) and diacylglycerol (DAG). DAG activates several processes including NFκB while IP3 facilities the entry of $Ca^{2+}$ into the cytoplasm culminating in NFAT translocation and transcriptional activation of target genes.[44] To evaluate changes in $Ca^{2+}$ flux in T cells during TCR stimulation we used total internal reflection fluorescence microscopy (TIRFM).[45] We utilized an artificial lipid bilayer to evaluate TCR synapse formation during TCR stimulation and measure $Ca^{2+}$ flux using $Ca^{2+}$ sensitive fluorescent dyes TIRFM system. After synapse formation, individual control and *CISH* KO T cells were followed over the course of 30 minutes and evaluated for $Ca^{2+}$ flux. We found a significant increase in the amplitude and duration of $Ca^{2+}$ flux in CISH KO T cells after synapse formation (Figure 5E). There was no difference in $Ca^{2+}$ flux between control and *CISH* KO T cells when TCR signaling was bypassed by addition of Ionomycin (Figure 5E). These data confirm that the effects of *CISH* KO are specific to TCR stimulus and are in line with the augmented levels of phosphorylated PLCγ-1 and SLP76.

Phosphorylation of PLCγ-1 and SLP76 propagates a signaling cascade culminating in the translocation of NFAT and NFκB into the nucleus and activation of the MAPK pathway.[46,47] We observed an increase in the amplitude and duration of both NFAT and NFκB translocation to the nucleus after TCR stimulation in *CISH* KO versus control T cells (Figure 5F). A slight increase in c-Jun levels was also observed in *CISH* KO T cells, which is notable as increased c-Jun expression confers resistance to CAR T cell exhaustion.[48] Consistent with increased TCR signaling, we observed enhanced phosphorylation of ERK in *CISH* KO T cells versus controls (Figure 5G). Surprisingly, while AKT phosphorylation generally increased after TCR stimulation, there was no difference between control and hyper-activated *CISH* KO T cells (Figure 5H). From these data, it appears that *CISH* KO results in increased PLCγ-1 but not AKT phosphorylation. We and others have observed that AKT activation after stimulation is largely associated with T cell maturation.[49,50] These insights offer a potential mechanism for the paradoxical enhancement of expansion and hyper-activation without associated maturation observed in *CISH* KO T cells. Thus, we propose a model where *CISH* preferentially blocks PLCγ1 signaling but AKT phosphorylation is unaffected, resulting in increased proliferation, function, and survival without altering maturation (Figure 5I).

## CISH regulates expression of activation makers and susceptibility to PD1 blockade

In unmanipulated TIL we observed that CISH was inversely expressed with several activation/exhaustion markers. To evaluate the role of *CISH* in regulating the expression of these activation/exhaustion markers, we analyzed gene expression in *CISH* KO T cells by scRNAseq. *CISH* KO Naïve $CD8^+$ T cells from 3 donors were cultured for a total of 10 days, rested overnight, and then TCR stimulated for 4 hours and analyzed by scRNAseq for population-based expression patterns. In concert with our previous findings, we found *CISH* KO in T cells resulted in a significant increase in *IFNG*, *TNF* and *IL2* gene expression (Figure 6A). Not surprisingly, when T cells were grouped into *IFNG* high (above median) and low (below median), we observed high levels of *41BB* (*TNFRSF9*) in $IFNG^{high}$ and not $IFNG^{low}$ group (Figure 6B). Conversely, when T cells were separated based upon *CISH* expression into $CISH^{high}$ (above median) and $CISH^{low}$ (below median), we found that

the CISH$^{high}$ subset exhibited significantly lower expression of *41BB* and *PDCD1*, while CISH$^{low}$ cells had high levels of *41BB* and *PDCD1*.

In order to determine the functional relevance of increased PD1 expression in the absence of CISH we employed the pmel-1 *Cish*$^{-/-}$ murine melanoma model that uses a TCR transgenic which recognizes both murine and human melanoma antigen gp100.[16] T cells from WT and *Cish* KO pmel-1 congenically marked thy1.1 splenocytes were enriched and adoptively transferred into syngeneic C57BL/6 bearing B16 melanomas that express their antigen hgp100. Eight days post ACT, T cells were extracted from tumors, and evaluated for PD1 and the congenic marker thy1.1 expression by flow cytometry. Here, we found that PD1 was expressed significantly higher in *Cish* KO T cells compared to wildtype littermates (Figure 6C). This observation suggested that *Cish* KO T cell therapy would further benefit from PD1 blockade. Using the same ACT approach, a subset of mice also received anti-PD1 or isotype control as indicated. Untreated mice, mice receiving isotype antibody or mice receiving anti-PD1 alone quickly succumbed to their tumors (Figure 6D). The ACT of WT *Cish* pmel-1 T cells conferred only a marginal improvement in tumor treatment, whereas both *Cish* KO or combination of pmel-1 WT with anti-PD1 antibody significantly slowed tumor growth compared to anti-PD1 alone. The combination of pmel-1 *Cish* KO and anti-PD1 resulted in profound tumor regression. Moreover, the combination of *Cish* KO T cells and anti-PD1 treatment resulted in long-term survival (Figure 6E). These findings indicate that inhibition of CISH may improve the outcome of PD1 inhibition and that unleashing the internal and external potential of neoantigen T cells may greatly enhance the effectiveness of adoptive immunotherapy.

## Discussion

Cancer immunotherapy offers the potential to use a patient's own immune cells to mediate the destruction of metastatic cancer. Residing in the patient's own lesions are tumor-specific T cells that have specificity for cancer cells. Despite the presence of these specific T cells, in many cases cancer growth continues unabated.[51] Adoptive transfer *ex vivo* stimulated TIL can result in tumor regression and extended survival in patients with melanoma.[52] Yet despite the promise of TIL therapy, and the abundance of TIL that are accessible within the tumor microenvironment, a significant proportion of patients receiving TIL fail to have durable tumor regression. The mechanisms by which tumor microenvironments (TME) suppress T cell function are multifaceted and complex. Low antigen density, reduced MHC expression by tumor cells, and more recently cell surface immune checkpoint engagement, are among the core extrinsic contributors to unproductive responses to TCR ligation, preventing the initiation of potent and sustained cytolytic responses by tumor resident T cells. Checkpoint inhibition has improved regression of metastatic melanoma,[53–55] underscoring the value of targeted approaches to increase and prolong the antigen-specific T cell response. Comparatively, the identification and therapeutic targeting of important T cell intrinsic checkpoint mechanisms is far less developed, owing in part to the previous inherent difficulties in drugging intracellular target proteins.

T cells within the tumor microenvironment have been reported to be in a chronic state of antigenic stimulation and express markers of activation/exhaustion such as CD39, 41BB,

TOX and PD1.[19,56] Surprisingly, we observed that CISH was inversely expressed with these established activation/exhaustion markers in tumor resident T cells. CISH expression was enriched in tumor-resident T cells and found to be induced by TCR-specific stimulation with maximal expression positively correlating with T cell maturation status. Despite overlap in associated cell surface markers, activation and exhaustion processes are highly distinct at the transcriptional and epigenetic levels. For example, PD1 expression is regulated by a series of enhancer and insulator elements that differentially interact with transcription factors distinct to the processes of activation and exhaustion.[57] In the present study we did not evaluate the TCR specificity or chronology of the biphasic expression of CISH and PD1 in tumor resident T cells, although it is plausible that CISH limits activation-induced expression of PD1 by way of global suppression of T cell activation but becomes uncoupled when the transcriptional program shifts to one governed by exhaustion. In the current study, we focused on the physiological importance of *CISH* in the context of activation of human T cells present in the TME.

While the inactivation and blockade of classical cell-surface immune checkpoint targets such as PD-1 is readily achievable through monoclonal antibody-based targeting, intracellular signaling molecules such as CISH have historically been difficult to modulate with comparable efficacy and specificity. The advent of targeted gene editing tools such as CRISPR/Cas9 have allowed for precise, efficient, and permanent gene inactivation in human T cells.[28] In the current study we developed a CRISPR/Cas9 editing strategy that enables efficient and precise genetic disruption of *CISH* in human T cells and used this capability to characterize the impact of *CISH* KO on T cell function. *CISH* KO human T cells exhibited enhanced cytokine production; both in magnitude and polyfunctionality after TCR stimulation. The transduction of TCRs specific to cancer-testis antigen NY-ESO-1 into PBL coupled with CISH deletion resulted in profound increase in specific effector cytokine production and relevant tumor killing. Based on these findings we adapted our CRISPR/Cas9 approach to clinical scale, cGMP-compatible production of *CISH* KO neoantigen specific TIL, demonstrating highly efficient (>95%) and reproducible *CISH* KO in T cells derived from the tumors of multiple patients. Functional assessment after CISH deletion in TIL from three GI cancer patients revealed a consistent enhancement in mutant neoantigen reactivity and that was not observed against naturally found wildtype antigens. This effector cytokine response was maximally higher (in some cases 5-fold more) and retained over several antigen dose titrations. Thus, genetic ablation of *CISH* not only increases the overall functionality of T cells but also enhances TIL sensitivity to antigenic stimulation by at least some antigens.

Neoantigen reactivity initially detected in isolated TIL can be ‘lost’ or diminished during the rapid expansion proceeding ACT. In at least one patient, we observed that CISH inactivation was sufficient to restore detectable neoantigen reactivity that was absent in control TIL after traditional REP. This apparent increase in functional avidity following CISH KO could be of critical value in TIL immunotherapy where tumors likely express low levels of neoantigen, and where small populations of T cells bearing a neoantigen specific TCR are unable to mount a productive response due to suppression by the TME or low functional avidity. Regarding the latter, we identified several patients where mutant p53 tetramer-positive T cell clones were present but lacked the ability to mount measurable responses in functional

assays. In this instance, CISH KO was sufficient to uncover functional reactivity in these TIL populations without altering the frequency of tetramer positive TIL.Although this outcome likely depends on the initial frequency of TCR-reactive T cells and the sensitivity of the functional assays employed, our data imply that *CISH* KO increases functional avidity of TIL to mutation-specific neoantigens, including common p53 antigens, which may enhance and broaden the utility of TIL ACT.

Advances in DNA sequencing has made personalized precision medicine an attainable possibility.[7] At present, however, there remain many logistical challenges facing neoantigen TIL therapy.[58] Access to universal hotspot mutations could obviate many of these limitations if reactivities could be consistently found in patients.[34] We found an enrichment of *CISH* expression in tumor resections lacking reactivity to hotspot *TP53* mutations. CISH *KO* did not alter tetramer-positive precursor frequency but did significantly enhance reactivity against mutant p53. The deletion of CISH in conjunction with the transduction of a TCR library targeting shared hotspot mutations and HLAs could enable the broader application of neoantigen adoptive immunotherapy.

In our study we found that the *CISH* KO in mature patient TIL not only unleashes neoantigen reactivity, but also initiates a hyper-activation program with a significant increase in metabolic activity and expansion. We and others have observed that increased activation is often associated with progressive maturation and functional *in vivo* senescence[59] and observed that AKT signaling plays a key role in that process.[49,60] Molecular dissection of these activation pathways revealed that CISH selectively inhibited PLC$\gamma$1. Subsequently, the deletion of CISH resulted in increased ERK, NFAT and NFAT activity but not AKT in human T cells. This selective uncoupling of activation and maturation by CISH deletion might give insights into these critical biological processes and potential therapies.

TIL express a number of characterized activation/exhaustion markers that have been the focus of much study.[18,61] We were surprised to observe that CISH was largely inversely expressed with these markers in minimally processed tumor derived T cells. Analysis of scRNAseq of CISH depleted T cells revealed that CISH-low cells had high levels of PD1 and in a preclinical model the tumor-specific CISH-deficient T cells had an increase in PD1 expression in the tumor. This increased PD1 expression in the absence of CISH raised the question whether the inhibition of PD-1 in CISH-deficient T cells could further enhance their anti-tumor responses and highlights the need for studies addressing the effects of CISH loss on both intratumoral TIL phenotype and the effects on the tumor microenvironment in general. We addressed this question using a pmel-1 Cish$^{-/-}$ murine melanoma model that uses a transgenic TCR that recognizes both murine and human melanoma antigen gp100. We found that the transfer of CISH-deficient T cells in combination with anti-PD-1 antibody resulted in a synergistic response, leading to a significant and durable tumor regression and complete survival of tumor-bearing mice out to more than 70 days. These findings indicate that removing or blocking the intrinsic suppression of the of neoantigen reactivity of T cells via both CISH and PD-1 checkpoint blockade may significantly enhance the efficacy of adoptive cell immunotherapy in the clinical setting. In addition, a secondary consequence of CISH ablation is the ability of CISH KO TIL to maintain expansion in the presence of limiting IL-2 *in vitro*. Given that lymphodepleting preconditioning is suspected

to improve ACT by reducing competition for limiting cytokine, further optimization of this protocol, or its use in combination with other approaches may eventually allow for reduced lymphodepletion and/or reduced need for systemic IL-2 administration, thereby greatly reducing toxicity and complications associated with current ACT protocols.

Patient safety is a key consideration with the development of any new ACT approach. From a genetic engineering standpoint, we vetted the fidelity of our CRISPR/Cas9 editing approach using both deep sequencing of computationally predicted OT sites, as well as genome-wide, unbiased GUIDE-seq in both T cells and patient-derived TIL. We detected no OT editing events using either method, inspiring confidence that our CRISPR reagents are highly specific to *CISH*, with minimized risk of genotoxicity resulting from off-target DSB induction. Separately, the increase in T cell functional avidity following CISH KO presents unique safety concerns that must be considered. For instance, autoimmune uveitis and vitiligo can occur in melanoma patients who respond following TIL ACT due to the expression of tumor antigens on retinal pigment epithelium and normal melanocytes.[62] Our previous work in a mouse melanoma model indicated that CISH can exacerbate such toxicities.[16] Thus, in the setting of melanoma where off-tumor toxicities are common, the risk of exacerbating such toxicities must be weighed in the context of prognosis and the availability of alternative therapies. Conversely, epithelial malignancies such as those of the gastrointestinal tract are appealing from a clinical standpoint due to a comparatively lower mutational load and overall poor immunogenicity. ACT may maximally benefit from increased functional avidity in this setting, while the lower overall TCR diversity in TIL from such tumors may reduce the probability of off-tumor toxicity, particularly when neoantigen selection is employed.[63] It should be noted, however, that cancer-associated mutations can occur in non-malignant tissues.[64,65] In theory, this could create the possibility for on-target, off-tumor cytotoxicity. However, due to the low frequency of mutation-bearing, non-cancerous cells it is unclear whether such a situation would elicit organ-level toxicity, particularly as a primary role of the immune system is removal of premalignant cells. As with all novel T cell and checkpoint immunotherapies, any downstream clinical application must minimize these risks and balance them against the potential benefit to each individual patient.

Our findings demonstrate that advances in gene editing can result in successful modification of fully mature TIL and reverse internal suppression of neoantigen reactivity, making them more functional, proliferative and susceptible to checkpoint blockade. We demonstrate we can efficiently and precisely inactivate CISH using CRISPR and improve the anti-tumor responses of T cells. To this end, these pre-clinical data are the foundation for a recently initiated human clinical trial entitled “A Study of Metastatic Gastrointestinal Cancers Treated with Tumor Infiltrating Lymphocytes in Which the Gene Encoding the Intracellular Immune Checkpoint CISH Is Inhibited Using CRISPR Genetic Engineering” (ClinicalTrials.gov Identifier NCT04426669). Results from this trial will hopefully shed light on the feasibility, safety and efficacy of novel checkpoint inhibition using neoantigen-selected, CRISPR genetically engineered *CISH* KO T cell therapy for solid tumors.

## Limitations of the Study

The data presented here demonstrate a clear role for CISH in limiting TIL neoantigen reactivity via a novel mechanism and we have made great efforts to mitigate potential confounders. However, one potential limitation in this study is that we were only able to evaluate TIL derived from GI cancer patients with resectable tumors. Inaccessible lesions or TIL that failed to expand after resection were not assessed here, nor did we assess TIL derived from indications beyond GI and melanoma. As CISH deletion enhances the functional avidity of PBL-derived T cells from healthy donors and uncovers neoantigen reactivity in TIL initially deemed unreactive, it is reasonable to consider our findings may be more broadly applicable, however subsequent work will be necessary to confirm this. Additional patient exclusion criteria can be located here (NCT04426669), but broadly patients with brain metastatic lesions and underlying autoimmune inflammatory disorders were not admitted into the study. It is unclear if or how these underlying conditions could alter the findings described here. While widely accepted and published, we utilized only one animal model system targeting non-immunogenic B16 melanoma. The role of Cish in other models is the subject of future studies.

## STAR Methods

### RESOURCE AVAILABILITY

**Lead contact—**Further information and requests for resources should be directed to and fulfilled by the lead contact, Dr. Douglas C. Palmer (palmerdc33@gmail.com)

**Materials availability—**This study did not generate new unique reagents.

#### Data and code availability

- Data from single cell and bulk RNA sequencing is deposited Y
- This paper does not report original code.
- Any additional information required to reanalyze the data reported in this paper is available from the lead contact upon request.

### EXPERIMENTAL MODEL AND SUBJECT DETAILS

**Animals—**C57BL/6 mice (obtained from Charles River Laboratories, Frederick, MD) of 6–8 weeks of age were used as recipient hosts for adoptive transfer unless otherwise indicated. pmel thy1.1 transgenic mice (B6.Cg-/Cy Tg [TcraTcrb] 8Rest/J) were used for adoptive cell transfer experiments. All mice were maintained under specific pathogen-free conditions.

**Cell lines—**Modified B16-mhgp100 (H-2Db), a mouse melanoma cell line, was transduced as previously described to express glycoprotein 100 (gp100) mutated to express human amino acid residues at positions 25–27 (EGS to KVP); this line was used as the tumor model.

**Primary Cell Cultures—**TILs, infusion TILs, and dendritic cells were generated as previously described.[66] Briefly, to generate TILs, surgically resected tumors were cut into

twenty-four fragments approximately 1–2 mm in size and each fragment was placed into a separate well of a 24-well plate containing 2 ml of complete media (CM) containing high dose IL-2 (6000 IU/ml, Chiron). CM comprised of RPMI media supplemented with 10% in-house human serum, 2 mM L-glutamine, 25 mM HEPES and 10 μg/ml gentamicin. TIL fragment culture was selected for treatment and thus underwent a rapid expansion procedure in gas permeable G-Rex100 flasks using irradiated PBMC at a ratio of 1 to 100 in 400 ml of 50/50 medium, supplemented with 5% human AB serum, 3000 IU/ml of IL-2, and 30 ng/ml of OKT3 antibody (Miltenyi Biotec). 50/50 media consisted of a 1 to 1 mixture of CM with AIM-V media. All cells were cultured at 37°C with 5% $CO_2$. Human tumor lines Cell lines were maintained in complete media DMEM (Gibco) with 10% FBS, 2-Mercaptoethanol, 1% glutamine and 1% penicillin–streptomycin.

## METHOD DETAILS

**Immunoblot analysis.—**Western blot analysis was performed using standard protocols. Proteins were separated by 4%–12% SDS-PAGE, followed by standard immunoblot analysis using anti–CISH and β-actin (Cell Signaling). In brief, for immunoblot quantifications, cells were resuspended in a total cell extraction buffer and kept on ice for 10 min followed by homogenization. Cells were then centrifuged at 20,000g for 20 min at 4°C to pellet cell debris. Detection of proteins was performed using secondary antibodies conjugated to horseradish peroxidase-HRP and the super signal west pico chemiluminescent substrate (Thermo Scientific-Pierce) or using the manufacturers recommendations using the Wes (ProteinSimple). All antibodies are listed in the Key Resources Table.

**TCR signaling assessment by Immunoblot analysis—**Control and CISH KO T cells were rested overnight without cytokine. 3e6 T cells were distributed for 4 different time points. T cells were stimulated by 10ug of CD3-Biotin antibody (Miltenyi Biotech Catalog#130-113-137) for 0, 2, 5 and 10 minutes. Proteines were isolated using 10X RIPA buffer (Cell signaling technology catalog#9806) and protease/phosphatase buffer (Cell signaling technology catalog#5872) according to the manufacturer's protocol. Proteins were analyzed using traditional western blotting. Phospho-ZAP70(Y493), phospho-LAT (Y171), Phospho-PLCgamma (Y783), Phospho-SLP76 (Y145), phospho-ERK, phospho-AKT (T308), PLCgamma and beta-actin antibodies were used to detect primary proteins. Detection of proteins was performed using secondary antibodies conjugated to horseradish peroxidase-HRP and the super signal west pico chemiluminescent substrate (Thermo Scientific-Pierce). All antibodies are listed in the Key Resources Table.

**Nuclear and cytoplasmic fraction analysis by Immunoblot—**Control and CISH KO T cells were rested over night with out cytokines. 5e6 cells were collected from each condition. T cells were stimulated using 10ug CD3-biotin antibody (Miltenyi Biotech Catalog#130-113-137) for 0, 10 and 20 minutes. Upon stimulation cells were subjected for fractionation. Cytoplasmic and nuclear fractions were isolated using Thermofisher's nuclear extraction kit (Catlog#78835). Manufacturer's protocol was followed. Nuclear fraction was subjected for western blot analysis. NFkB and c-Jun were detected. Lamin A/C was used as loading control. All antibodies are listed in the Key Resources Table.

**Retroviral transduction.:** To produce the γ-retrovirus, package cell line 293GP were cotransfected with 9 μg of target vector DNA and 4 μg envelope plasmid (RD114 envelope was used to produce virus to infect human T cells; pEco envelope was used to produce virus to infect murine T cells) using lipofectamine 2000 (Cat. No. 11668019, Invitrogen, Carlsbad, California, USA) on a 100 $mm^2$ poly-D-lysine–coated plate (Corning, New York, USA). Viral supernatants were harvested 48 and 72 hours after transfection. For T-cell transduction, human peripheral blood mononuclear cells were activated with 50 ng/mL OKT3 (Cat. No. 130-093-387, Miltenyi Biotec) and harvested for retroviral transduction on day 2. Cells were applied to vector-preloaded RetroNectin (Takara) coated non-tissue culture 6-well plates (Corning) at a concentration of $1\times10^6$ per well and centrifuged at 1500rpm at 32°C for 10 minutes. After centrifugation, the cells were then cultured in AIM-V medium containing 10% human AB serum (Valley Biomedical) and 300 IU/mL IL-2 until use.

**Peripheral blood T cell editing with CRISPR/Cas9.:** PBL T cells were stimulated using anti-CD3/CD28 dynabeads in X-Vivo 15 supplemented with 10% human AB serum, 300IU/ml IL-2, and 5 ng/mL IL-7 and IL-15 for 48 hours prior to electroporation. T cells were electroporated with 15ug Cas9 mRNA and 10ug CISH sgRNA using the Neon electroporator (3e6 in 100ul tip) and pulse conditions 1400V, 10ms, 3 pulses. Electroporated T cells were recovered in T cell media without antibiotics for 30min before bringing to 1e6/ml in complete T cell media.

**Genomic DNA Analysis—**Genomic DNA was isolated from engineered T cells and TIL at 7- or 14-days post electroporation, respectively, by spin column-based purification (Qiagen). Isolated genomic DNA was subject to PCR amplification of the genomic regions surrounding the CISH gRNA target locus. CRISPR/Cas9 editing efficiency was analyzed at the genomic level by Sanger sequencing of the PCR amplicons, and subsequent analysis of the Sanger sequencing traces using Tracking of Indels by Decomposition (TIDE) (https://tide.nki.nl/)[29] TIDE is a web-based algorithm to determine the frequency and size of insertions and deletions resulting from CRISPR/Cas9 DSB induction based on comparison of Sanger trace from a control and experimental sample. Indel frequncy at computationally predicted off-target (OT) loci was evaluated by PCR using locus-specific primers (Table S1) and amplicon sequencing by next-generation sequencing (NGS).

**Production of *CISH* KO TIL using CRISPR/Cas9.:** Interleukin-2 expanded tumor infiltrating lymphocytes (TIL) were thawed (day −5) and allowed to recover for 24 hours in TIL medium (X-Vivo 15, 10% human AB serum, 6000 IU/mL IL-2, and 5 ng/mL IL-7 and IL-15) at 37°C, 5% $CO_2$. After the initial rest period (day −4), TIL cultures were harvested and a volume reduction step was performed prior to re-suspension in fresh TIL media followed by stimulation with plate bound (5 μg/ml) anti-CD3 (OKT3) and soluble anti-CD28 (2 μg/mL) for 4 days at 37°C, 5% $CO_2$. Four days later (day 0), stimulated TIL were washed with PBS and re-suspended at $2.5\times10^7$ NC/mL in either PBS (GMP process) or Neon buffer T. Each $2.5\times10^6$ viable TIL were electroporated with 15μg Cas9 mRNA and 10μg *CISH* gRNA (GGGTTCCATTACGGCCAGCG) in a 100μl tip using the Neon electroporation device (Life Technologies) using parameters 1400v, 10 ms width, 3 pulses.

For non-REP expansion, TIL were immediately returned to TIL medium and maintained at ~1 × $10^6$ viable cells/ml with either media addition or 50% volume exchange as required.

**Rapid expansion of *CISH KO* TIL.:** For rapid expansion protocol (REP), electroporated TIL were immediately transferred to TIL REP media (X-Vivo 15, 5% human AB serum, 3000 IU/mL IL-2) and seeded at 5 – 7.5 × $10^3$ viable TIL per $cm^2$ in G-Rex culture vessels (Wilson Wolf, New Brighton MN) and combined with either autologous or allogeneic (3 pooled donors) irradiated PBMC feeders at a ratio of 1 TIL to 100 feeders (1:100). G-Rex vessels were incubated for 6–8 days at 37°C, 5% $CO_2$. On day 6–8, the culture was evaluated and split according to the following: if viable NC/mL < 1 × $10^6$ VNC/mL, a 1:3 split was performed; if viable NC/mL ≥ 1 × $10^6$ VNC/mL, a 1:6 split was performed. Each G-Rex was equally transferred to 2 or 5 additional vessels according to split criteria above and fresh expansion media was added. All vessels were incubated for an additional 6–8 days at 37°C, 5% $CO_2$.

**Neoantigen screening.:** Tumors from cancer patients were surgically resected at the NIH Clinical Center and subjected to whole-exomic sequencing to identify non-synonymous somatic mutations. TIL cultures derived from individual tumor fragments from a single metastatic colon lesion were initially screened for reactivity against multiple TMG constructs or peptide pools using the enzyme-linked immunospot (ELISPOT) assay and flow cytometric evaluation of up-regulation of the T cell activation marker 4–1BB as previously described.[7]

**Intracellular Cytokine Staining (ICS).:** To evaluate the functionality of *CISH* KO T cells they were assayed for specific release of functional cytokines in a co-culture with neoantigen loaded APCs. APCs, either B cells or DCs as indicated, were generated from autologous PBMCs and cultured for 5 days. Concurrently, the cryo-preserved gene-modified cells from were thawed in pre-warmed complete media supplemented with IL-2 (300 IU/mL) and grown for 2 days. On the day of the co-culture, APCs were pulsed with mutant or wildtype (WT) peptides for 2 hours and then washed prior to being mixed with either *CISH* KO T cells or Control T cells. The co-culture was setup in the presence of golgi-blocking reagents and allowed to continue for 6 hours. After the 6 hours, samples were extracellular stained for T cell makers, fixed and permeabilized, then stained for the cytokines IFN-γ, IL-2 and TNF-α. Flow cytometry was then performed, and cells were analyzed for specific function.

**Cytotoxicity.:** Cytotoxicity assays were carried out with the IncuCyte S3-Platform (Essen BioScience). Adherent 526 (HLA-$A2^+$NY-ESO-$1^-$) or 624 (HLA-$A2^+$NY-ESO-$1^+$) tumor cells were plated at 1 × $10^4$ cells per well and incubated overnight at 37°C/5% CO2 in RPMI-1640 medium supplemented with 10% heat-inactivated FBS and GlutaMAX (Life Technologies) in a 96-well flat-bottom plate. The next day, cells were washed and incubated with indicated numbers of NY-ESO-1 TCR-transduced T cells from either control or CISH KO and 3.3 μmol/L IncuCyte Caspase-3/7 reagent (Essen BioScience). Cells were imaged at times indicated to detect apoptosis. Data were analyzed using IncuCyte S3 software (Essen BioScience) to distinguish apoptotic tumor cells from apoptotic T cells.

**GUIDE-seq.:** GUIDE-seq analysis was performed as described previously using a 6-mismatch cutoff (1), with the following modifications for application to primary lymphocytes. PBL T cells and TIL were stimulated using anti-CD3/CD28 dynabeads for 36–48 hours prior to electroporation in T cell media supplemented with IL-2 (300 IU/ml for PBL-T, and 3000IU/ml for TIL), 5ng/ml IL-7, and 5ng/ml IL-15. Cells were electroporated with 15ug Cas9 mRNA, 10ug CISH sgRNA, and 8–16pmol of GUIDE-seq dsODN using the Neon electroporator at 3e6/100ul tip and pulse conditions 1400V, 10ms, 3 pulses. On-target integration of dsDNA oligo was confirmed by PCR and TIDE (Tracking of Indels by Decomposition) analysis prior to NGS.

**GSEA.:** Gene set enrichment was analyzed using GSEA software (http://software.broadinstitute.org/gsea/downloads.jsp). Pathway Analysis was performed on the identified differentially expressed genes list using the Core Analysis function included in Ingenuity Pathway Analysis (IPA, Qiagen).

**scRNAseq Capture and library preparation.:** Single cell suspensions were prepared for single cell RNA-Seq partitioning, barcoding and library generation on the 10x Genomics Chromium platform. Suspensions were washed twice by pelleting cells with centrifugation at 300g in a chilled spinning bucket centrifuge and gentle resuspension in fresh ice-cold PBS with 0.04% BSA. Cell concentrations and viability were determined on a LunaFL fluorescent cell counter using Acridine Orange and Propidium Iodide dye (Logo Biosystems). Suspension concentrations were adjusted and loaded onto the Chromium microfluidic chip using the 3’ v3 gene expression chemistry to target 6,000 barcoded cells, and in samples where fewer cells were available, at the full concentration. Reverse transcription, cDNA amplification, and sequencing library preparation was all performed according to vendor’s user guide.

**Sequencing and primary data processing.:** Sequencing of final single cell RNA-Seq libraries was performed with the NCI-CCR Genomics Core on the NextSeq 500 platform using 150-cycle v2.5 High Output reagents with a 28bp read for identifying cell-specific barcode and UMI sequences, a 8bp index read for multiplexed sample identity, and a 98bp read to identify the cDNA insert. Multiplexed samples were sequenced multiple times to achieve target read depth. Data was processed with the 10x Genomics cellranger v3.0.1 pipeline to generate sample fastq sets followed by alignment of reads to the human GRCh38 reference sequence prepared by 10x Genomics (refdata-cellranger-GRCh38–3.0.0), generation of a cell barcode by expressed gene matrix, and basic quality metrics of capture, library and sequencing performance. The gene matrices from the 10X Genomics Cell Ranger were filtered by removing duplicated cells, dead cells, cells with low gene counts, and non-informative genes with zero-count across all samples. The data were normalized by R package Seurat version 2.3.4, visualized with R package Rtsne version 0.13, and clustered using the graph-based algorithm, Louvain, in R package igraph version 1.0.0. The gene-gene expression correlation was calculated with the mean-expression value of genes in 101 clusters using the generalized linear model (glm) for p-value and the spearman correlation for R-squared value. Expression violin plots were created on the high and low

expression groups based on the expression value above and below the mean along with t-test p-values.

**Supported lipid bilayer (SLB) and calcium flux measurement.:** Liposomes containing 6.25% DGS-NTA and 2% Cap-Biotin-DOPC lipids were prepared using an extruder method as per manufacturer's instruction (Avanti Polar Lipids, Inc.). Briefly, liposomes were applied to charged cover glasses for about 30 to form planar bilayer. The lipid bilayer was washed with HBS BSA buffer and then incubated with streptavidin (5mg/ml) for 30 min at RT and then with mono-biotinylated anti-CD3 antibody (1μg/ml OKT3, eBiosciences), histidine tagged CD80 (100 molecules/$\mu m^2$), and ICAM-1 (100 molecules/$\mu m^2$). Finally, the SLB was washed and brought to 37°C before injecting the cells. Calcium flux measurement was done according to the protocol as described by Skokos et al 2007. WT or CISH KO T cells were labeled with 2μM Fura-2-Am in serum free HBS buffer for 30 min at room temperature followed by de-esterification of the dye for another 30 min at 37°C in serum containing buffer. Imaging of cells was performed using 40X 1.35NA UApo 340 objective. Images of cells were acquired at a distance of 3 mm from the interference reflection microscopy image plane to acquire fluorescence from the equatorial plane of the cell. Cells were imaged live at 37°C while interacting with the SLB in HBS buffer containing $Ca^{2+}$ and $Mg^{2+}$. The Fura-2 emission at 510 nm upon excitation with both 340 and 380 nm light was captured for a few fields of cells. These fields of cells were repeatedly imaged for 40 min to obtain a time course of multiple cells. At the end of the experiment cells were treated with a buffer containing 1 μM Ionomycin, 20 mM Calcium and 2mM Magnesium to record the high calcium condition followed by a treatment with a buffer containing 3mM Magnesium, 2mM EGTA and no calcium to record the low calcium condition. Image analysis was performed using Metamorph software.

**Metabolomics.:** T cells from 6 donors were flash frozen before or after 4 hours of stimulation with CD3 crosslinking. Samples were then analyzed for metabolites using Metabolons inhouse services. The present human dataset comprises a total of 251 compounds of known identity (named biochemicals). Following normalization to DNA concentration, log transformation and imputation of missing values, if any, with the minimum observed value for each compound, Paired *t*-tests and Welch's two-sample *t*-test were used to identify biochemicals that differed significantly between experimental groups. For OCR, T cells were measured at 37°C using an Xfe96 extracellular analyzer (Seahorse Bioscience). Briefly, $10^6$ cultured T cells were initially plated on poly-L-Lysine coated XF96 well plate in unbuffered DMEM (DMEM with 25 mM glucose as indicated, 1 mM sodium pyruvate, 32 mM NaCl, 2 mM GlutaMax, pH 7.4) and incubated in a non-CO2 incubator for 30 minutes at 37°C. OCR was calculated using Seahorse XFe-96 proprietary software.

## QUANTIFICATION AND STATISTICAL ANALYSIS

**Statistics.—**Significance was determined by either student *t* test or ANOVA for repeated measures, *P <0.05, **P<0.01, ***P<0.001, ****P<0.0001. No assumptions were made regarding the data prior too analysis, analysis was not blinded and no samples were excluded from analysis.

## Supplementary Material

Refer to Web version on PubMed Central for supplementary material.

## Acknowledgements

This study was funded by Intima Bioscience. U.S., and in part through the Intramural program CCR at the National Cancer Institute. Support from CCR Single Cell Analysis Facility was funded by FNLCR Contract HSN261200800001E. Sequencing was performed with the CCR Genomics Core. This work utilized the computational resources of the NIH HPC Biowulf cluster. (http://hpc.nih.gov) Next generation sequencing and bioinformatic analysis of CRISPR off-target activity was conducted at the University of Minnesota Genomics Center (UMGC).

### Declaration of Interests

M.C. is a co-founder of Intima Bioscience. B.R.W, S.A.R, and B.S.M have received sponsored research support from Intima Bioscience. D.C.P., B.R. W, M.C., S.A.R., B.S.M, and N.P.R. have patents filed based on the findings described here.

## References

1. Heslop HE, Ng CY, Li C, Smith CA, Loftin SK, Krance RA, Brenner MK, and Rooney CM (1996). Long-term restoration of immunity against Epstein-Barr virus infection by adoptive transfer of gene-modified virus-specific T lymphocytes. Nat. Med 2, 551–555. [PubMed: 8616714]
2. Ilyas S, and Yang JC (2015). Landscape of Tumor Antigens in T Cell Immunotherapy. J. Immunol 195, 5117–5122. [PubMed: 26589749]
3. McGranahan N, Furness AJS, Rosenthal R, Ramskov S, Lyngaa R, Saini SK, Jamal-Hanjani M, Wilson GA, Birkbak NJ, Hiley CT, et al. (2016). Clonal neoantigens elicit T cell immunoreactivity and sensitivity to immune checkpoint blockade. Science 351, 1463–1469. [PubMed: 26940869]
4. Rizvi NA, Hellmann MD, Snyder A, Kvistborg P, Makarov V, Havel JJ, Lee W, Yuan J, Wong P, Ho TS, et al. (2015). Cancer immunology. Mutational landscape determines sensitivity to PD-1 blockade in non-small cell lung cancer. Science 348, 124–128. [PubMed: 25765070]
5. Samstein RM, Lee C-H, Shoushtari AN, Hellmann MD, Shen R, Janjigian YY, Barron DA, Zehir A, Jordan EJ, Omuro A, et al. (2019). Tumor mutational load predicts survival after immunotherapy across multiple cancer types. Nat. Genet 51, 202–206. [PubMed: 30643254]
6. Zhao J, Chen AX, Gartrell RD, Silverman AM, Aparicio L, Chu T, Bordbar D, Shan D, Samanamud J, Mahajan A, et al. (2019). Immune and genomic correlates of response to anti-PD-1 immunotherapy in glioblastoma. Nat. Med 25, 462–469. [PubMed: 30742119]
7. Robbins PF, Lu Y-C, El-Gamil M, Li YF, Gross C, Gartner J, Lin JC, Teer JK, Cliften P, Tycksen E, et al. (2013). Mining exomic sequencing data to identify mutated antigens recognized by adoptively transferred tumor-reactive T cells. Nat. Med 19, 747–752. [PubMed: 23644516]
8. Tran E, Ahmadzadeh M, Lu Y-C, Gros A, Turcotte S, Robbins PF, Gartner JJ, Zheng Z, Li YF, Ray S, et al. (2015). Immunogenicity of somatic mutations in human gastrointestinal cancers. Science 350, 1387–1390. [PubMed: 26516200]
9. Gros A, Parkhurst MR, Tran E, Pasetto A, Robbins PF, Ilyas S, Prickett TD, Gartner JJ, Crystal JS, Roberts IM, et al. (2016). Prospective identification of neoantigen-specific lymphocytes in the peripheral blood of melanoma patients. Nat. Med 22, 433–438. [PubMed: 26901407]
10. Tran E, Turcotte S, Gros A, Robbins PF, Lu Y-C, Dudley ME, Wunderlich JR, Somerville RP, Hogan K, Hinrichs CS, et al. (2014). Cancer immunotherapy based on mutation-specific CD4+ T cells in a patient with epithelial cancer. Science 344, 641–645. [PubMed: 24812403]
11. Zacharakis N, Chinnasamy H, Black M, Xu H, Lu Y-C, Zheng Z, Pasetto A, Langhan M, Shelton T, Prickett T, et al. (2018). Immune recognition of somatic mutations leading to complete durable regression in metastatic breast cancer. Nat. Med 24, 724–730. [PubMed: 29867227]
12. Anderson SC, Cooper AB, Jensen OP, Minto C, Thorson JT, Walsh JC, Afflerbach J, Dickey-Collas M, Kleisner KM, Longo C, et al. (2017). Improving estimates of population status and trend with superensemble models. Fish Fish 18, 732–741.

13. Ohashi J, Naka I, Patarapotikul J, Hananantachai H, Looareesuwan S, and Tokunaga K (2002). Significant association of longer forms of CCTTT Microsatellite repeat in the inducible nitric oxide synthase promoter with severe malaria in Thailand. J. Infect. Dis 186, 578–581. [PubMed: 12195390]

14. Palmer SE, Marre O, Berry MJ 2nd, and Bialek W (2015). Predictive information in a sensory population. Proc. Natl. Acad. Sci. U. S. A 112, 6908–6913. [PubMed: 26038544]

15. Khor CC, Vannberg FO, Chapman SJ, Guo H, Wong SH, Walley AJ, Vukcevic D, Rautanen A, Mills TC, Chang K-C, et al. (2010). CISH and susceptibility to infectious diseases. N. Engl. J. Med 362, 2092–2101. [PubMed: 20484391]

16. Palmer DC, Guittard GC, Franco Z, Crompton JG, Eil RL, Patel SJ, Ji Y, Van Panhuys N, Klebanoff CA, Sukumar M, et al. (2015). Cish actively silences TCR signaling in CD8+ T cells to maintain tumor tolerance. J. Exp. Med 212, 2095–2113. [PubMed: 26527801]

17. Sanchez-Taltavull D, Perkins TJ, Dommann N, Melin N, Keogh A, Candinas D, Stroka D, and Beldi G (2020). Bayesian correlation is a robust gene similarity measure for single-cell RNA-seq data. NAR Genom Bioinform 2, lqaa002. [PubMed: 33575552]

18. Alfei F, Kanev K, Hofmann M, Wu M, Ghoneim HE, Roelli P, Utzschneider DT, von Hoesslin M, Cullen JG, Fan Y, et al. (2019). TOX reinforces the phenotype and longevity of exhausted T cells in chronic viral infection. Nature 571, 265–269. [PubMed: 31207605]

19. Schietinger A, Philip M, Krisnawan VE, Chiu EY, Delrow JJ, Basom RS, Lauer P, Brockstedt DG, Knoblaugh SE, Hämmerling GJ, et al. (2016). Tumor-Specific T Cell Dysfunction Is a Dynamic Antigen-Driven Differentiation Program Initiated Early during Tumorigenesis. Immunity 45, 389–401. [PubMed: 27521269]

20. Sekine T, Perez-Potti A, Rivera-Ballesteros O, Strålin K, Gorin J-B, Olsson A, Llewellyn-Lacey S, Kamal H, Bogdanovic G, Muschiol S, et al. (2020). Robust T Cell Immunity in Convalescent Individuals with Asymptomatic or Mild COVID-19. Cell 183, 158–168.e14. [PubMed: 32979941]

21. Blank R, Barnett AL, Cairney J, Green D, Kirby A, Polatajko H, Rosenblum S, Smits-Engelsman B, Sugden D, Wilson P, et al. (2019). International clinical practice recommendations on the definition, diagnosis, assessment, intervention, and psychosocial aspects of developmental coordination disorder. Dev. Med. Child Neurol 61, 242–285. [PubMed: 30671947]

22. Kurtulus S, Madi A, Escobar G, Klapholz M, Nyman J, Christian E, Pawlak M, Dionne D, Xia J, Rozenblatt-Rosen O, et al. (2019). Checkpoint Blockade Immunotherapy Induces Dynamic Changes in PD-1-CD8+ Tumor-Infiltrating T Cells. Immunity 50, 181–194.e6. [PubMed: 30635236]

23. Gros A, Robbins PF, Yao X, Li YF, Turcotte S, Tran E, Wunderlich JR, Mixon A, Farid S, Dudley ME, et al. (2014). PD-1 identifies the patient-specific $CD8^+$ tumor-reactive repertoire infiltrating human tumors. J. Clin. Invest 124, 2246–2259. [PubMed: 24667641]

24. Hendel A, Bak RO, Clark JT, Kennedy AB, Ryan DE, Roy S, Steinfeld I, Lunstad BD, Kaiser RJ, Wilkens AB, et al. (2015). Chemically modified guide RNAs enhance CRISPR-Cas genome editing in human primary cells. Nat. Biotechnol 33, 985–989. [PubMed: 26121415]

25. Doench JG, Fusi N, Sullender M, Hegde M, Vaimberg EW, Donovan KF, Smith I, Tothova Z, Wilen C, Orchard R, et al. (2016). Optimized sgRNA design to maximize activity and minimize off-target effects of CRISPR-Cas9. Nat. Biotechnol 34, 184–191. [PubMed: 26780180]

26. Sanson KR, Hanna RE, Hegde M, Donovan KF, Strand C, Sullender ME, Vaimberg EW, Goodale A, Root DE, Piccioni F, et al. (2018). Optimized libraries for CRISPR-Cas9 genetic screens with multiple modalities. Nat. Commun 9, 5416. [PubMed: 30575746]

27. Goff DC, Hill M, and Freudenreich O (2010). Strategies for improving treatment adherence in schizophrenia and schizoaffective disorder. J. Clin. Psychiatry 71 Suppl 2, 20–26. [PubMed: 21190649]

28. Osborn MJ, Webber BR, Knipping F, Lonetree C-L, Tennis N, DeFeo AP, McElroy AN, Starker CG, Lee C, Merkel S, et al. (2016). Evaluation of TCR Gene Editing Achieved by TALENs, CRISPR/Cas9, and megaTAL Nucleases. Mol. Ther 24, 570–581. [PubMed: 26502778]

29. Brinkman EK, Chen T, Amendola M, and van Steensel B (2014). Easy quantitative assessment of genome editing by sequence trace decomposition. Nucleic Acids Res. 42, e168. [PubMed: 25300484]

30. Lu Y, Xue J, Deng T, Zhou X, Yu K, Deng L, Huang M, Yi X, Liang M, Wang Y, et al. (2020). Safety and feasibility of CRISPR-edited T cells in patients with refractory non-small-cell lung cancer. Nat. Med 26, 732–740. [PubMed: 32341578]

31. Stadtmauer EA, Fraietta JA, Davis MM, Cohen AD, Weber KL, Lancaster E, Mangan PA, Kulikovskaya I, Gupta M, Chen F, et al. (2020). CRISPRengineered T cells in patients with refractory cancer. Science 367. Available at: 10.1126/science.aba7365.

32. Tsai SQ, Zheng Z, Nguyen NT, Liebers M, Topkar VV, Thapar V, Wyvekens N, Khayter C, Iafrate AJ, Le LP, et al. (2015). GUIDE-seq enables genome-wide profiling of off-target cleavage by CRISPR-Cas nucleases. Nat. Biotechnol 33, 187–197. [PubMed: 25513782]

33. Yossef R, Tran E, Deniger DC, Gros A, Pasetto A, Parkhurst MR, Gartner JJ, Prickett TD, Cafri G, Robbins PF, et al. (2018). Enhanced detection of neoantigen-reactive T cells targeting unique and shared oncogenes for personalized cancer immunotherapy. JCI Insight 3. Available at: 10.1172/jci.insight.122467.

34. Malekzadeh P, Pasetto A, Robbins PF, Parkhurst MR, Paria BC, Jia L, Gartner JJ, Hill V, Yu Z, Restifo NP, et al. (2019). Neoantigen screening identifies broad TP53 mutant immunogenicity in patients with epithelial cancers. J. Clin. Invest 129, 1109–1114. [PubMed: 30714987]

35. Abbas AR, Baldwin D, Ma Y, Ouyang W, Gurney A, Martin F, Fong S, van Lookeren Campagne M, Godowski P, Williams PM, et al. (2005). Immune response in silico (IRIS): immune-specific genes identified from a compendium of microarray expression data. Genes Immun. 6, 319–331. [PubMed: 15789058]

36. Lugli E, Kvistborg P, and Galletti G (2019). Cancer neoantigens targeted by adoptive T cell transfer: private no more. J. Clin. Invest 129, 949–951. [PubMed: 30714989]

37. Lo W, Parkhurst M, Robbins PF, Tran E, Lu Y-C, Jia L, Gartner JJ, Pasetto A, Deniger D, Malekzadeh P, et al. (2019). Immunologic Recognition of a Shared p53 Mutated Neoantigen in a Patient with Metastatic Colorectal Cancer. Cancer Immunology Research 7, 534–543. Available at: 10.1158/2326-6066.cir-18-0686. [PubMed: 30709841]

38. Lanzavecchia A, and Sallusto F (2002). Progressive differentiation and selection of the fittest in the immune response. Nat. Rev. Immunol 2, 982–987. [PubMed: 12461571]

39. Gattinoni L, Lugli E, Ji Y, Pos Z, Paulos CM, Quigley MF, Almeida JR, Gostick E, Yu Z, Carpenito C, et al. (2011). A human memory T cell subset with stem cell-like properties. Nat. Med 17, 1290–1297. [PubMed: 21926977]

40. Zhu H, Blum RH, Bernareggi D, Ask EH, Wu Z, Hoel HJ, Meng Z, Wu C, Guan K-L, Malmberg K-J, et al. (2020). Metabolic Reprograming via Deletion of CISH in Human iPSC-Derived NK Cells Promotes In Vivo Persistence and Enhances Anti-tumor Activity. Cell Stem Cell 27, 224–237.e6. [PubMed: 32531207]

41. Guittard G, Dios-Esponera A, Palmer DC, Akpan I, Barr VA, Manna A, Restifo NP, and Samelson LE (2018). The Cish SH2 domain is essential for PLC-γ1 regulation in TCR stimulated CD8+ T cells. Sci. Rep 8, 5336. [PubMed: 29593227]

42. Houtman JCD, Houghtling RA, Barda-Saad M, Toda Y, and Samelson LE (2005). Early phosphorylation kinetics of proteins involved in proximal TCR-mediated signaling pathways. J. Immunol 175, 2449–2458. [PubMed: 16081816]

43. Wange RL, and Samelson LE (1996). Complex complexes: signaling at the TCR. Immunity 5, 197–205. [PubMed: 8808675]

44. Courtney AH, Lo W-L, and Weiss A (2018). TCR Signaling: Mechanisms of Initiation and Propagation. Trends Biochem. Sci 43, 108–123. [PubMed: 29269020]

45. Varma R, Campi G, Yokosuka T, Saito T, and Dustin ML (2006). T cell receptor-proximal signals are sustained in peripheral microclusters and terminated in the central supramolecular activation cluster. Immunity 25, 117–127. [PubMed: 16860761]

46. Gaud G, Lesourne R, and Love PE (2018). Regulatory mechanisms in T cell receptor signalling. Nat. Rev. Immunol 18, 485–497. [PubMed: 29789755]

47. Voisinne G, Kersse K, Chaoui K, Lu L, Chaix J, Zhang L, Goncalves Menoita M, Girard L, Ounoughene Y, Wang H, et al. (2019). Quantitative interactomics in primary T cells unveils TCR signal diversification extent and dynamics. Nat. Immunol 20, 1530–1541. [PubMed: 31591574]

48. Lynn RC, Weber EW, Sotillo E, Gennert D, Xu P, Good Z, Anbunathan H, Lattin J, Jones R, Tieu V, et al. (2019). c-Jun overexpression in CAR T cells induces exhaustion resistance. Nature 576, 293–300. [PubMed: 31802004]
49. Crompton JG, Sukumar M, Roychoudhuri R, Clever D, Gros A, Eil RL, Tran E, Hanada K-I, Yu Z, Palmer DC, et al. (2015). Akt inhibition enhances expansion of potent tumor-specific lymphocytes with memory cell characteristics. Cancer Res. 75, 296–305. [PubMed: 25432172]
50. Pollizzi KN, Patel CH, Sun I-H, Oh M-H, Waickman AT, Wen J, Delgoffe GM, and Powell JD (2015). mTORC1 and mTORC2 selectively regulate $CD8^+$ T cell differentiation. J. Clin. Invest 125, 2090–2108. [PubMed: 25893604]
51. Spranger S, Luke JJ, Bao R, Zha Y, Hernandez KM, Li Y, Gajewski AP, Andrade J, and Gajewski TF (2016). Density of immunogenic antigens does not explain the presence or absence of the T-cell-inflamed tumor microenvironment in melanoma. Proc. Natl. Acad. Sci. U. S. A 113, E7759–E7768. [PubMed: 27837020]
52. Anderson KG, Stromnes IM, and Greenberg PD (2017). Obstacles Posed by the Tumor Microenvironment to T cell Activity: A Case for Synergistic Therapies. Cancer Cell 31, 311–325. [PubMed: 28292435]
53. Brahmer JR, Tykodi SS, Chow LQM, Hwu W-J, Topalian SL, Hwu P, Drake CG, Camacho LH, Kauh J, Odunsi K, et al. (2012). Safety and activity of anti-PD-L1 antibody in patients with advanced cancer. N. Engl. J. Med 366, 2455–2465. [PubMed: 22658128]
54. Topalian SL, Hodi FS, Brahmer JR, Gettinger SN, Smith DC, McDermott DF, Powderly JD, Carvajal RD, Sosman JA, Atkins MB, et al. (2012). Safety, activity, and immune correlates of anti-PD-1 antibody in cancer. N. Engl. J. Med 366, 2443–2454. [PubMed: 22658127]
55. Topalian SL, Hodi FS, Brahmer JR, Gettinger SN, Smith DC, McDermott DF, Powderly JD, Sosman JA, Atkins MB, Leming PD, et al. (2019). Five-Year Survival and Correlates Among Patients With Advanced Melanoma, Renal Cell Carcinoma, or Non-Small Cell Lung Cancer Treated With Nivolumab. JAMA Oncol 5, 1411–1420. [PubMed: 31343665]
56. Baitsch L, Baumgaertner P, Devêvre E, Raghav SK, Legat A, Barba L, Wieckowski S, Bouzourene H, Deplancke B, Romero P, et al. (2011). Exhaustion of tumor-specific $CD8^+$ T cells in metastases from melanoma patients. J. Clin. Invest 121, 2350–2360. [PubMed: 21555851]
57. Bally APR, Austin JW, and Boss JM (2016). Genetic and Epigenetic Regulation of PD-1 Expression. J. Immunol 196, 2431–2437. [PubMed: 26945088]
58. Coulie PG, Van den Eynde BJ, van der Bruggen P, and Boon T (2014). Tumour antigens recognized by T lymphocytes: at the core of cancer immunotherapy. Nat. Rev. Cancer 14, 135–146. [PubMed: 24457417]
59. Gattinoni L, Klebanoff CA, Palmer DC, Wrzesinski C, Kerstann K, Yu Z, Finkelstein SE, Theoret MR, Rosenberg SA, and Restifo NP (2005). Acquisition of full effector function in vitro paradoxically impairs the in vivo antitumor efficacy of adoptively transferred CD8+ T cells. J. Clin. Invest 115, 1616–1626. [PubMed: 15931392]
60. Klebanoff CA, Crompton JG, Leonardi AJ, Yamamoto TN, Chandran SS, Eil RL, Sukumar M, Vodnala SK, Hu J, Ji Y, et al. (2017). Inhibition of AKT signaling uncouples T cell differentiation from expansion for receptor-engineered adoptive immunotherapy. JCI Insight 2. Available at: 10.1172/jci.insight.95103.
61. Simoni Y, Becht E, Fehlings M, Loh CY, Koo S-L, Teng KWW, Yeong JPS, Nahar R, Zhang T, Kared H, et al. (2018). Bystander CD8+ T cells are abundant and phenotypically distinct in human tumour infiltrates. Nature 557, 575–579. [PubMed: 29769722]
62. Yeh S, Karne NK, Kerkar SP, Heller CK, Palmer DC, Johnson LA, Li Z, Bishop RJ, Wong WT, Sherry RM, et al. (2009). Ocular and systemic autoimmunity after successful tumor-infiltrating lymphocyte immunotherapy for recurrent, metastatic melanoma. Ophthalmology 116, 981–989.e1. [PubMed: 19410956]
63. Tran E, Robbins PF, and Rosenberg SA (2017). “Final common pathway” of human cancer immunotherapy: targeting random somatic mutations. Nat. Immunol 18, 255–262. [PubMed: 28198830]

64. Lawson ARJ, Abascal F, Coorens THH, Hooks Y, O'Neill L, Latimer C, Raine K, Sanders MA, Warren AY, Mahbubani KTA, et al. (2020). Extensive heterogeneity in somatic mutation and selection in the human bladder. Science 370, 75–82. [PubMed: 33004514]

65. Lee-Six H, Olafsson S, Ellis P, Osborne RJ, Sanders MA, Moore L, Georgakopoulos N, Torrente F, Noorani A, Goddard M, et al. (2019). The landscape of somatic mutation in normal colorectal epithelial cells. Nature 574, 532–537. [PubMed: 31645730]

66. Tran E, Robbins PF, Lu Y-C, Prickett TD, Gartner JJ, Jia L, Pasetto A, Zheng Z, Ray S, Groh EM, et al. (2016). T-Cell Transfer Therapy Targeting Mutant KRAS in Cancer. N. Engl. J. Med 375, 2255–2262. [PubMed: 27959684]

## Highlights

- CISH is associated with non-functional tumor-infiltrating lymphocytes (TIL)
- CISH KO uncovers TIL neoantigen reactivity
- CISH KO induces hyper-activation but not hyper-maturation
- Cish KO synergizes with PD1 blockade *in vivo*

**Context and Significance:**

The inconsistent success of therapies based on tumor-infiltrating lymphocytes (TIL) recognizing “neoantigens” (tumor-specific targets) has been the focus of intense study. Authors from the National Cancer Institute and University of Minnesota describe a key role for the Cytokine-induced SH2 protein (CISH) in regulating human T cell function and reactivity to neoantigens. To explore the functional and mechanistic base of these findings, the authors developed an efficient, clinical-grade process to eliminate CISH in primary human TIL. CISH deficiency increased TIL function and neoantigen recognition. In a preclinical *in vivo* model, CISH knockout also increased tumor vulnerability to checkpoint inhibition (a type of cancer immunotherapy). This work served as the basis for a first-in-human clinical trial of CISH knockout TIL in patients with metastatic gastrointestinal cancers.

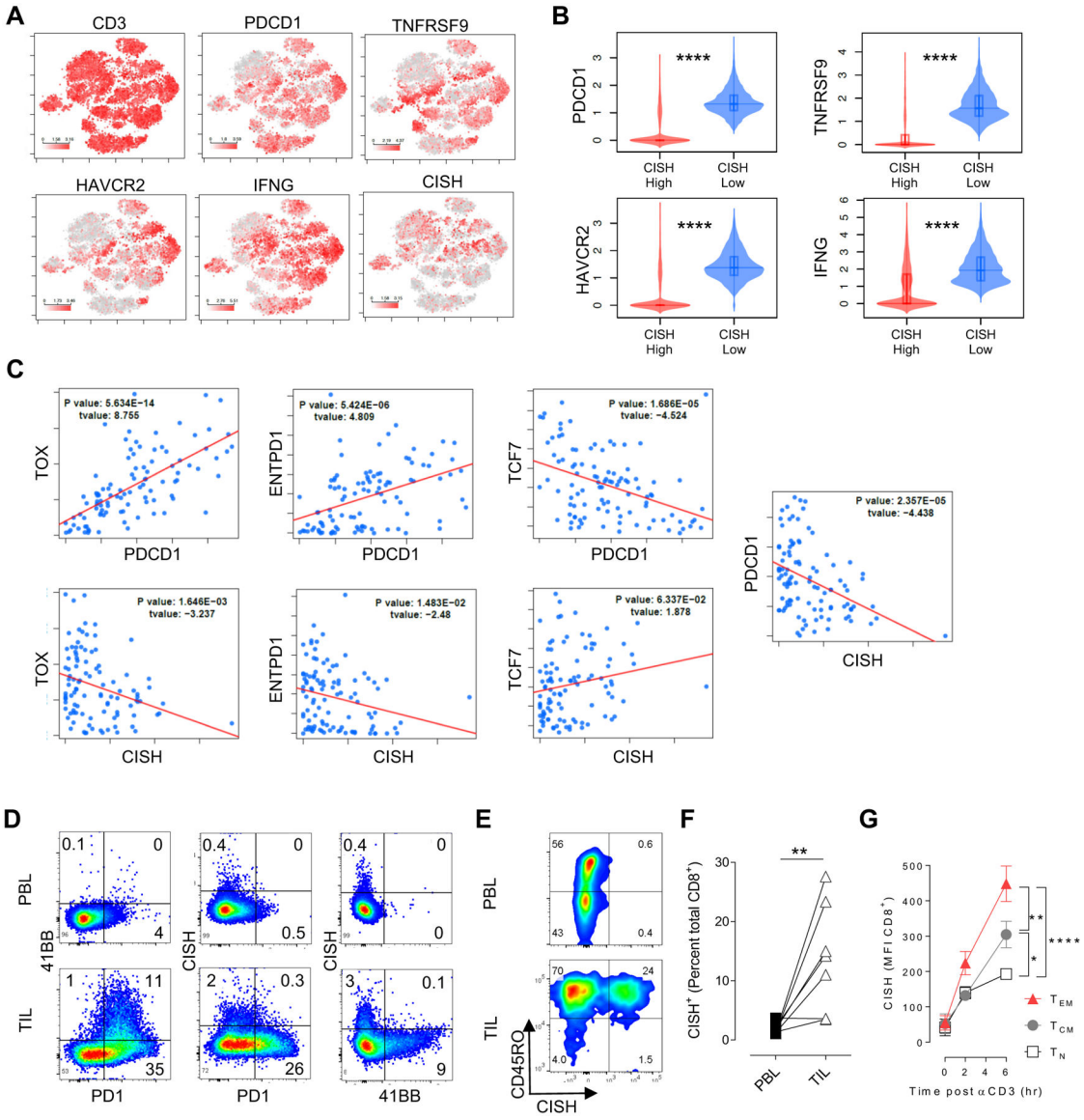


**Fig. 1. CISH is inversely expressed with markers of activation/exhaustion in melanoma patient-derived TILs.**

**A-C**, scRNAseq from tumor-derived T cells reveals unique clustering of CISH with other known effector/exhaustion markers. T cells were enriched from fresh tumor resections and subjected to scRNAseq (n=7 biological replicates). **B**, Violin plots of effector genes from median CISH high (>50%) of median CISH low (<50%) T cells from scRNAseq. **C**, Cluster analysis of TIL scRNAseq reveals CISH is expression is inverse to key markers of activation/exhaustion. T-value indicates positive (>1) or negative (<1) correlation. **D**, Differential expression of CISH, PD1 and 41BB in TIL. Fresh tumor resections and patient matched PBL were evaluated for co-expression of CISH, PD1 and 41BB on $CD3^+$ T cells by flow cytometry. Representative of 3 patients. **E**, Flowcytometric evaluation of CISH expression in $CD8^+$ T cells from PBL or matched tumor resections. **F**, Summary of increased expression of CISH in T cells from TIL tumors relative to matched PBL. n = 7 melanoma patients. **G**, Increased induction of CISH after TCR stimulation in naive $CD8^+$

T cells (N), Central Memory CD8+ T ($T_{CM}$), Effector Memory $CD8^+$ T cells ($T_{EM}$). n = 4 healthy donors. $T_N$, Naïve ($CD62L^+CD45RO^-$); $T_{CM}$, Central Memory ($CD62^+CD45RO^+$); $T_{EM}$, Effector Memory ($CD62L^-CD45RO^+$). Statistical significance was determined by student *t* test, **P<0.01. Error bars denote +/−SEM.

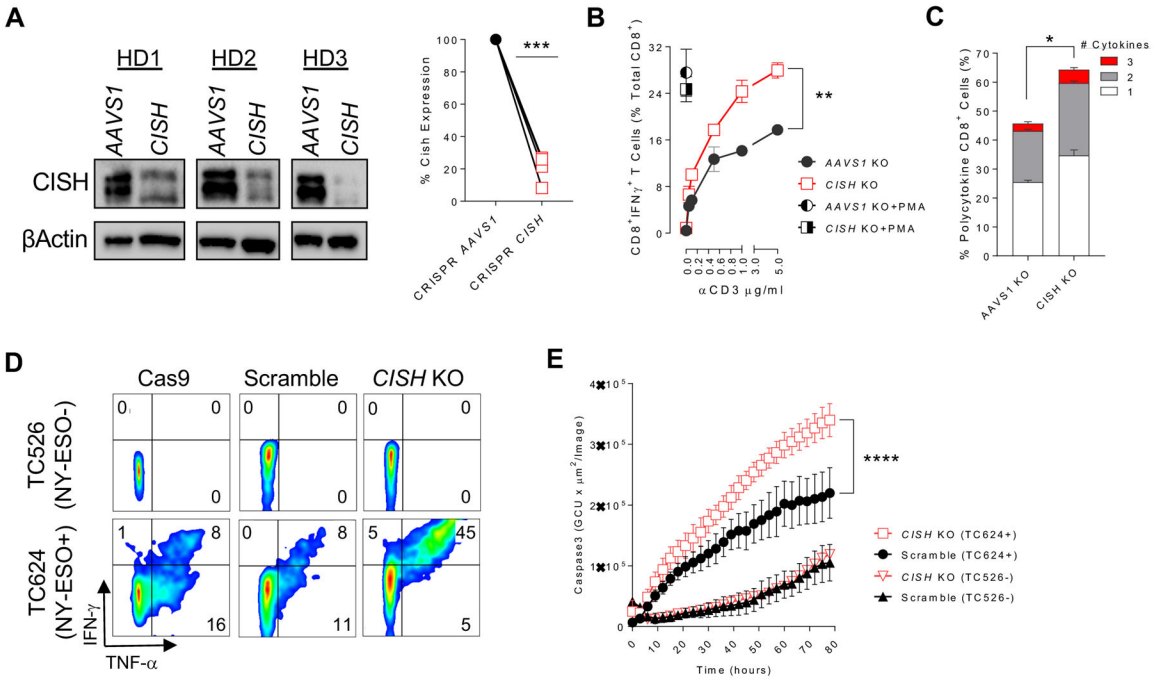


**Fig. 2. Efficient Knockout of *CISH* and hyperactivation in mature T cells.**

**A**, Significant reduction of CISH protein in T cells from 3 donors after CRISPR by Western blot densitometry relative to βactin. **B**, Enhanced polyfunctionality after CISH deletion. Evaluation of IFN-γ, TNF-α and IL2 after CD3 stimulation and ICS. 1, 2, or 3 indicates the number of cytokines concurrently detected. **C,** Significant enhancement in tumor reactivity after CISH deletion. Co-culture and ICS of NY-ESO-1-specific TCR transduced T cells and CRISPR of CISH with tumors expressing NY-ESO-1 (TC624) or without (TC526). **D**, Significant increase in tumor cell killing by CISH knockout T cells. Live tumor killing from (**C**) using activation of caspase3 substrate and live tumor imagining over time. (**B-C**), representative of 3 independent donors, (**D**) representative of two donors. Statistical significance was determined by either student *t* test or ANOVA for repeated measures, *P <0.05, **P<0.01, ***P<0.001, ****P<0.0001. Error bars denote +/−SEM.

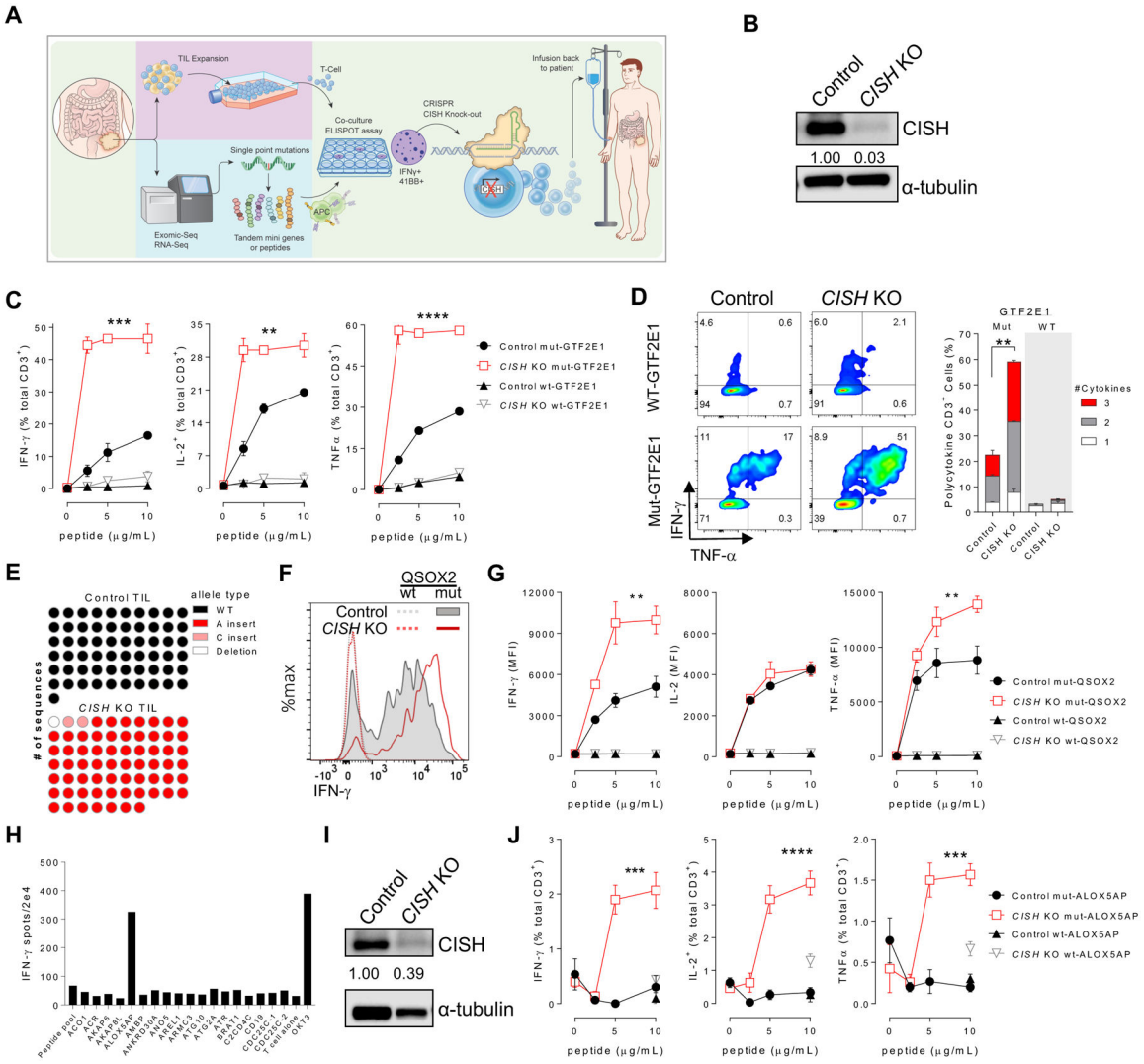


**Fig. 3. Enhanced neoantigen reactivity after the deletion of CISH in TIL.**

**A**, Schematic for GMP production of CISH deficient TIL. The tumor is split after excision. In one fragment T cells are grown out and in the other fragment the tumor is subjected to exomic and RNA sequencing. Non-synonymous point-mutations predicted to bind to autologous MHC are made into tandem mini genes or peptides targets. T cells derived from the tumor resection and neoantigen loaded autologous APCs are then co-cultured and assayed for the upregulation of IFN-γ or 41BB. Reactive wells are then stimulated and subjected to CRISPR mediated knockout of CISH. **B**, patient A, efficient knockout of *CISH* post CRISPR in mature TIL and evaluated by immunoblot analysis. **C**, *CISH* ko increased cytokine production and polyfunctionality after co-culture with wildtype (WT) and neoantigen loaded APCs as determined by ICS in patient A. (**D**) Evaluation of polyfunctionality of neoantigen reactive T cells after deletion of CISH in T cells co-cultured with targets in patient A. Cytokines evaluated include IFN-γ, TNF-α, and IL-2. **E**, Evaluation of CRISPR-induced disruptions in the CISH locus by Sanger sequencing in patient B. All Indels detected result in alternate coding and premature termination prior to the functional SH2 and SOCS domains. **F**, CISH deletion increased intensity of cytokine

production on a per cell basis after co-culture with neoantigen loaded APCs and subjected to ICS in patient B. **G**, Significant increase in MFI of IFN-γ and TNF-α against neoantigens after CISH deletion in TIL and coculture of titrated neoantigen loaded APCs in patient B. **H**, Patient C had initial neoantigen reactivity that was lost after expansion. Initial coculture of T cells from a tumor fragment with potential neoantigen loaded APCs and assayed by IFN-γ ELISpot. **I**, Immunoblot analysis for CISH following stimulation and CRISPR mediated KO of CISH. **J**, Neoantigen reactivity was "restored" after CISH deletion in TIL and cocultured with neoantigen loaded APCs and assayed by ICS. Statistical significance was determined by either student *t* test or ANOVA for repeated measures, *P <0.05, **P<0.01, ***P<0.001, ****P<0.0001. Error bars denotes +/−SEM.

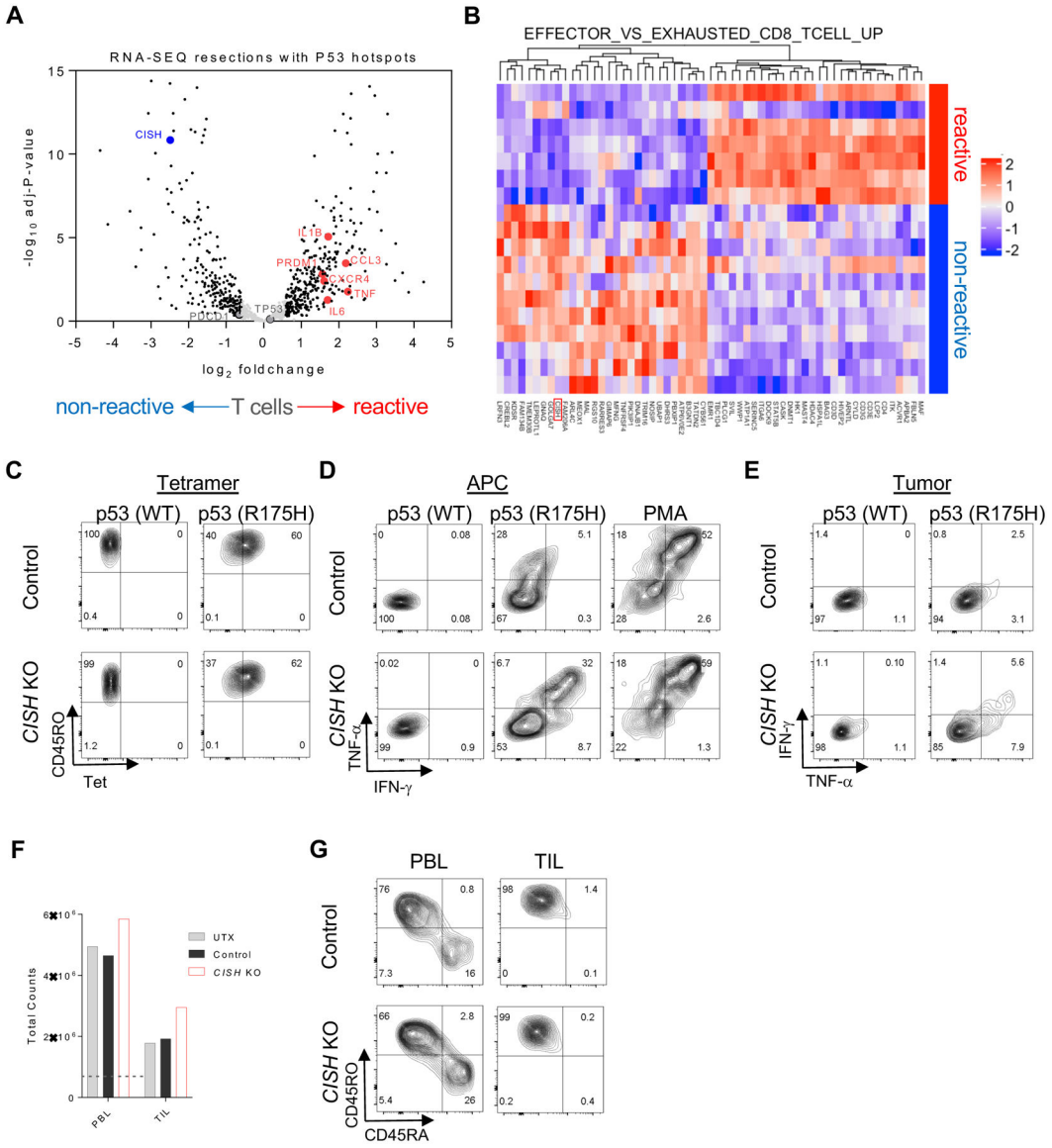


**Fig. 4. CISH KO restores TIL reactivity against universal hotspot p53 mutations.**

**A**, Immunological gene signature expression analysis from tumor fragments with p53 hotspot mutations that were found to have or not have detectable T cell reactivity to mutant p53. Fresh tumor fragments were sequenced for p53 hotspot mutations. 18 fragments were identified to contain known targetable p53 neoantigens. Isolated TIL from each fragment were screened for p53 neoantigen reactivity, 7 fragments were found to have p53 hotspot reactivity, while 11 did not. Volcano plot of immune-filtered genes from RNA-SEQ of tumor resections from reactive and non-reactive cultures. Gray indicates genes below 1.5-fold change and/or a p>0.05. **B**, Cluster analysis of differentially expressed immunological genes associated with effector and exhausted phenotype in $CD8^+$ T cells. Each row represents an individual tumor fragment and are clustered into TIL with and without reactivity to mutant p53. **C**, WT p53 or mutant p53 (R175H) tetramer staining of TIL from patient D with or without CISH deletion. **D**, Significant increase in IFN-γ and TNF-α against p53 hotspot

mutation after CISH deletion in TIL cocultured with antigen-loaded APCs and assayed by ICS. **E**, Augmented tumor reactivity after CISH deletion. Increase in IFN-γ and TNF-α staining in CISH deleted TIL cocultured with p53 hotspot mutation expressing tumors and assayed by ICS. **F**, Cell count of PBL and matched TIL from patient D after CISH deletion and 10 days of culture. Dotted line indicates initial starting count. **G**, Flow cytometric evaluation of phenotype of PBL or TIL from patient D after CISH deletion after 10 days of culture. Statistical significance was determined by either student *t* test or ANOVA for repeated measures, *P <0.05, **P<0.01, ***P<0.001, ****P<0.0001. Error bars denotes +/−SEM.

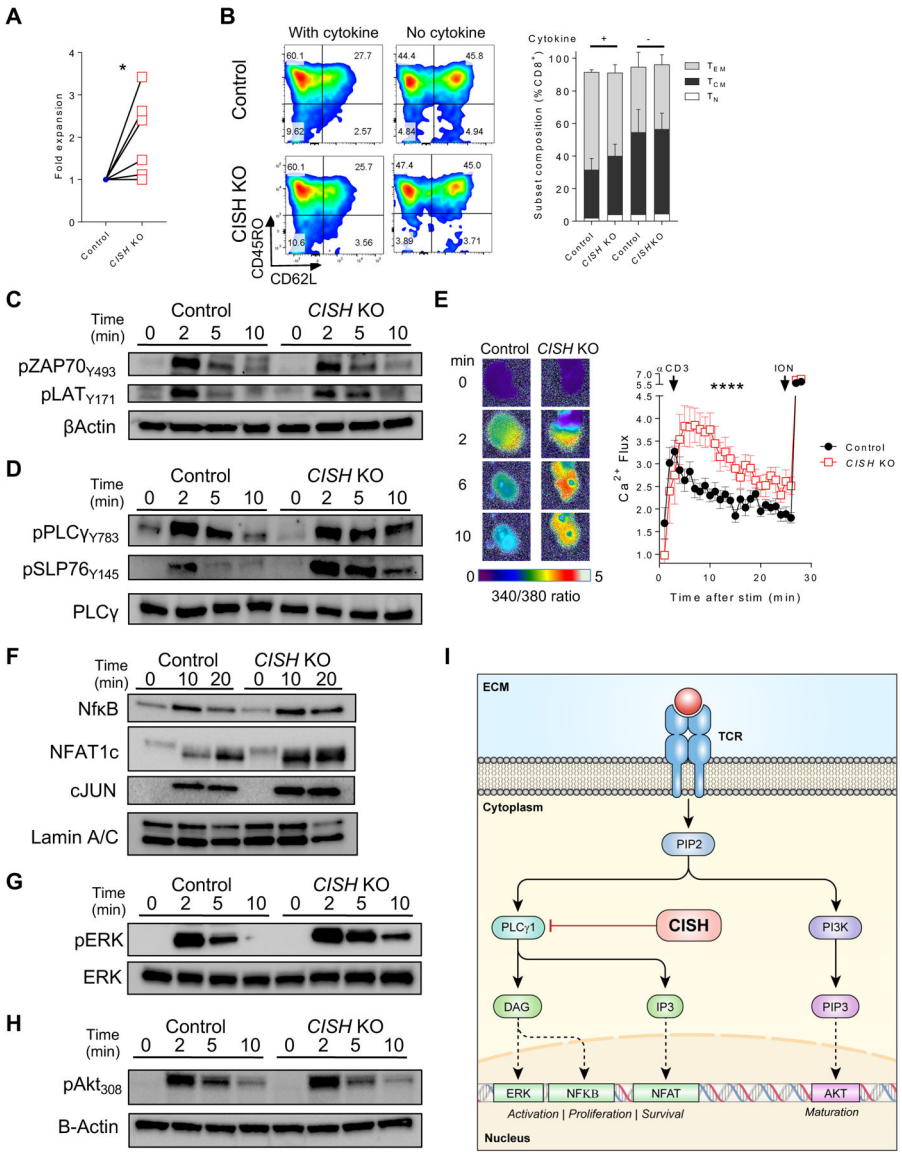


**Fig. 5. CISH KO increases T cell activation but not maturation.**

**A**, CISH deletion results in increased T cell expansion. Following naïve $CD8^+$ T cell enrichment, T cells were TCR stimulated, CISH deleted by CRISPR mediated KO and evaluated for expansion. Relative fold-change in T cell expansion compared to non-deleted controls after 14 days of culture ($n$=7 biological replicates). **B**, CISH deletion does not alter T cell maturation. Phenotypic analysis by flow cytometry of naïve-derived $CD8^+$ CISH deleted T cells with TCR stimulation and supportive cytokines or with TCR alone after 14 days of culture. No significant difference was observed in the composition of T cell subsets after CISH deletion in either condition. $T_N$, Naïve ($CD62L^+CD45RO^-$); $T_{CM}$, Central Memory ($CD62^+CD45RO^+$); $T_{EM}$, Effector Memory ($CD62L^-CD45RO^+$). **C-hH**, CISH deletions results in hyperactivation of intermediate and late TCR signaling components. Naïve-derived $CD8^+$ T cells deleted for CISH and cultured for 10 days. T cells were rested overnight and were re-stimulated with cross-linked αCD3 and immunoblotted or evaluated

for $Ca^{2+}$ flux at times indicated. **C**, CISH deletion does not alter early TCR signaling. Immunoblot analysis for $pZAP70_{Y493}$, $pLAT_{Y171}$, and βActin at times indicated with or without CISH KO. **D**, CISH inhibits intermediate TCR signaling. Immunoblot analysis for pPLCγ1Y783, pSLP76Y145, and whole PLCγ1 after TCR ligation at times indicated with or without CISH KO. **E**, Increased $Ca^{2+}$ flux after CISH deletion and TCR-ligation using TIRF microscopy on a lipid bilayer. Individual T cells with or without CISH deletion were followed for $Ca^{2+}$ flux at times indicates after forming immunological synapses. (n=13–18 T cells per group). **F**, CISH deletion enhances nuclear translocation of NFκB and NFAT after TCR ligation. Immunoblot analysis for nuclear NFκB, NFAT1c, c-JUN and Lamin A/C after TCR ligation at times indicated with or without CISH KO. **G-H**, CISH deletions results in hyperactivation of ERK but not AKT. Immunoblot analysis for pERK and whole ERK after TCR ligation at times indicated with or without CISH KO. **H**, Immunoblot analysis for $pAKT_{S473}$ and β-actin after TCR ligation at times indicated with or without CISH KO. **I**, Proposed model of how CISH may regulate T cell activation, proliferation and survival but not maturation through PLCγ1 and not AKT signaling. Representative of 3 independent donors. Statistical significance was determined by either student *t* test or ANOVA for repeated measures, *P <0.05, **P<0.01, ***P<0.001, ****P<0.0001. Error bars denotes +/−SEM.

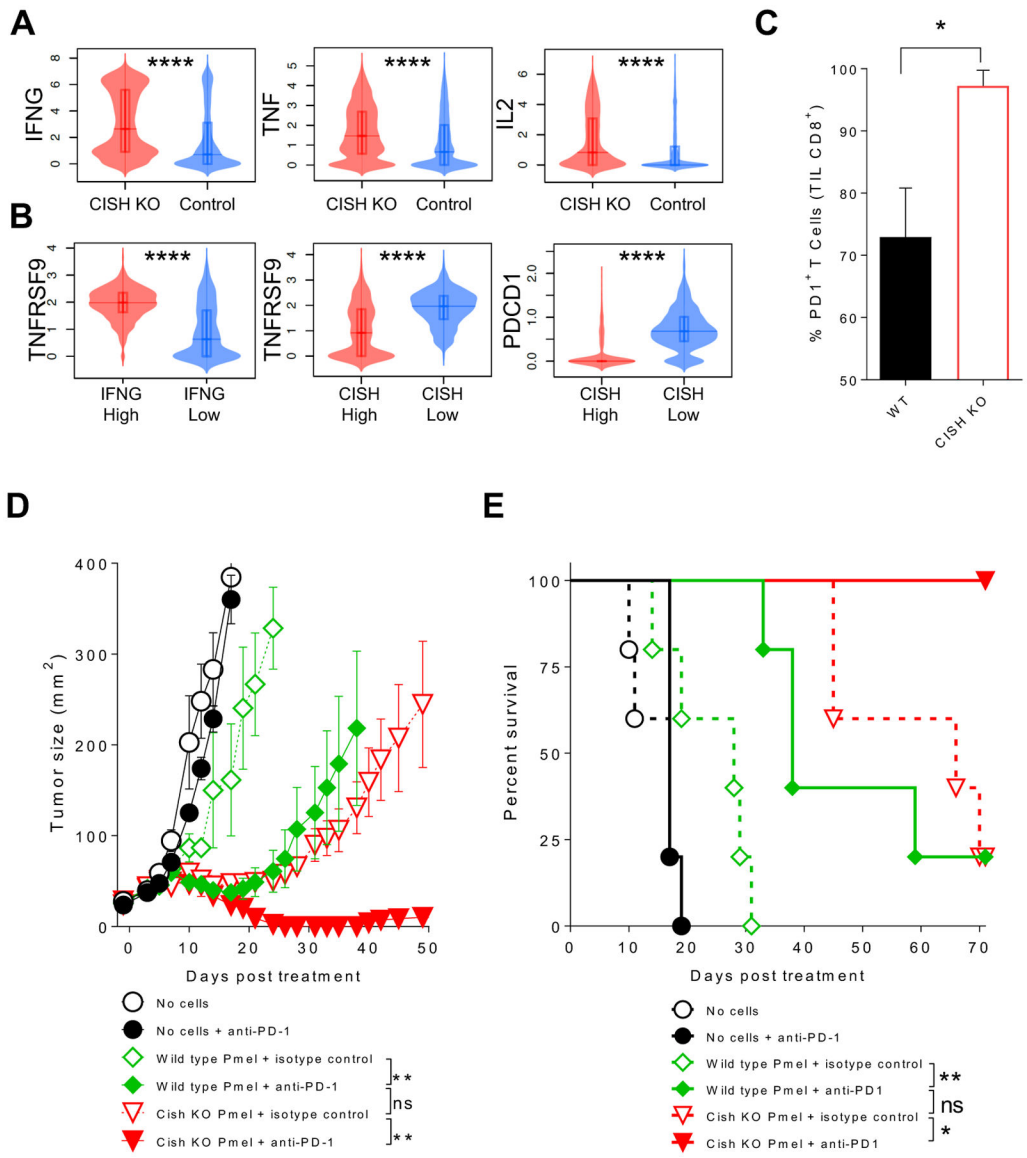


**Fig. 6. CISH KO unleashes and activation program and susceptibility to PD1 blockade**

**A-B**, CISH deletion increases cytokine production and 41BB and PD1 expression. **A**, Violin plots for IFNG, TNF, IL2 gene expression from scRNAseq of T cells with or without CISH deletion 4 hours after TCR stimulation (n=3 biological replicates). **B**, Violin plots of effector genes from median IFNG or CISH high (>50%) of median IFNG or CISH low (<50%) T cells from scRNAseq of CISH deleted TCR stimulated T cells. **C**, Increased PD1 expression in TIL knocked out for CISH. Flow cytometry analysis of murine $CD8^+$ TIL seven days after adoptive cell transfer (ACT) of naïve melanoma-specific T cells knocked out for CISH. **D-E** Combination of CISH deletion and PD1 blockade significantly enhances adoptive immunotherapy. Adoptive cell transfer (ACT) of melanoma-specific T cells knocked out for Cish into B16-melanoma bearing mice with or without administration of antibodies blocking PD1 blockade. Product of perpendicular diameters blindly evaluated over time, 5 mice per group, independently repeated 3 times. **E**, Survival of mice treated in **D**. Statistical

significance was determined by either student *t* test, ANOVA for repeated measures, or Log-Rank Mantel-Cox test, *P <0.05, **P<0.01, ***P<0.001, ****P<0.0001.

Key resources table

| REAGENT or RESOURCE | SOURCE | IDENTIFIER |
|---|---|---|
| **Antibodies** | | |
| Anti-CISH | Cell Signaling | 8731S |
| Anti-beta actin | Cell Signaling | 8457S |
| OKT3 | Miltenyi | 130-093-387 |
| anti-CD28 | Invitrogen | 16028985 |
| Anti-IFN-γ | eBioscience | 48-7319-42 |
| Anti-IL2 | eBioscience | 25-7029-42 |
| Anti- TNF-α | eBioscience | 17-7349-82 |
| pAkt (Ser473) | Cell Signaling | 4060 |
| pAkt (Thr308) | Cell Signaling | 13038 |
| Phospho ZAP70 (Y493) | Cell Signaling | 2704 |
| Phospho LAT (Y145) | Cell Signaling | 3581 |
| TCF7 | Cell Signaling | 2203S |
| Phospho PLCγ (Y783) | Cell Signaling | 14008S |
| PLCγ | Cell Signaling | 5690S |
| Phospho SLP76 (Y145) | Cell Signaling | 14770S |
| Phospho ERK (Thr202/Tyr204) | Cell Signaling | 4370S |
| ERK | Cell Signaling | 4695S |
| βActin | Cell Signaling | 3700 |
| Nf-κB | Cell Signaling | 8242S |
| NFAT1c | Cell Signaling | 5861S |
| LEF1 | Cell Signaling | 2230S |
| LAMIN A/C | Cell Signaling | 4777 |
| αRabbit HRP | Cell Signaling | 7074S |
| αMouse HRP | Cell Signaling | 7076S |
| **Bacterial and virus strains** | | |
| Gamma retrovirus | In house | N/A |
| **Biological samples** | | |
| Tumors from cancer patients | NIH Clinical Center | N/A |
| Tumor infiltrating lymphocytes (TIL) | In house | N/A |
| Autologous B cells | In house | N/A |
| Autologous Dendritic cells | In house | N/A |
| Infusion TILs | In house | N/A |
| Peripheral blood mononuclear cells | In house | N/A |
| Neoantigen loaded APCs | In house | N/A |
| CISH KO T-cells | In house | N/A |
| PBL T-cells | In house | N/A |

| REAGENT or RESOURCE | SOURCE | IDENTIFIER |
|---|---|---|
| **Chemicals, peptides, and recombinant proteins** | | |
| IL-2 | PeproTech | 200-02 |
| IL-7 | PeproTech | 200-07 |
| IL-15 | PeproTech | 200-15 |
| Human AB serum | Valley Biomedical | HP1022HI |
| Super signal west pico chemiluminescent substrate | ThermoFisher | 35050061 |
| Lipofectamine 2000 | Invitrogen | 11668019 |
| RetroNectin | Takara | T202 |
| Wild type peptides | ih house | N/A |
| Mutant peptides | inhouse | N/A |
| GlutaMAX | Life Technologies | 35050061 |
| Fetal bovine serum | Peak Serum | PS-FB1 |
| IncuCyte Caspase-3/7 reagent | Essen BioScience | 4440 |
| Acridine Orange / Propidium Iodide Stain | Logo Biosystems | F23001 |
| NextSeq 500/550 150-cycle v2.5 High Output reagents | Illumina | 20024907 |
| histidine tagged CD80 | in house | N/A |
| ICAM-1 | Sino Biological | 50440-M08H-20 |
| **Critical commercial assays** | N/A | N/A |
| **Deposited data** | | |
| 10x Genomics scRNA matrices | This paper | https://github.com/CBIIT-CGBB/CISH_Cell_Med |
| **Experimental models: Cell lines** | | |
| B16-mhgp100 (H-2Db) mouse melanoma line | in house | |
| package cell line 293GP | ATCC | CRL-3215 |
| 526 (HLA-A2$^{+}$NY-ESO-1$^{-}$) tumor cells | in house | N/A |
| 624 (HLA-A2$^{+}$NY-ESO-1$^{+}$) tumor cells | in house | N/A |
| | | |
| **Experimental models: Organisms/strains** | | |
| C57BL/6 mice | NCI-Charles River Laboratories | N/A |
| pmel thy1.1 transgenic mice | in house and Jackson Labs | 005023 |
| **Oligonucleotides** | | |
| *CISH* gRNA: GGGTTCCATTACGGCCAGCG | Trilink Biotechnologies | N/A |
| GUIDE-seq dsODN (sense- 5′-P-G*T*TTAATTGAGTTGTCATATGTTAATAACGGT*A*T-3′ antisense- 5′-P-A*T*ACCGTTATTAACATATGACAACTCAATTAA*A*C-3′) | Integrated DNA Technologies | N/A |
| **Recombinant DNA** | | |
| Envelope plasmid (RD114) | In House | N/A |
| pEco envelope | In House | N/A |
| RD114 | Addgene | 17576 |
| **Software and algorithms** | | |

| REAGENT or RESOURCE | SOURCE | IDENTIFIER |
|---|---|---|
| Tracking of Indels by Decomposition (TIDE) | Webtool | https://tide.nki.nl/ |
| FlowJo | BD Life Sciences | version 10.7.1 |
| IncuCyte S3 software | Essen BioScience | N/A |
| GSEA software | Broad Institute | http://software.broadinstitute.org/gsea |
| Ingenuity Pathway Analysis | Qiagen | |
| 10x Genomics cellranger | 10x Genomics | v3.0.1 pipeline |
| refdata-cellranger-GRCh38-3.0.0 reference | 10x Genomics | v3.0.0 |
| R package Seurat | R project | version 2.3.4 |
| R package Rtsne | R project | version 0.13 |
| R package igraph | R project | version 1.0.0 |
| Metamorph software | Molecular Devices | N/A |
| Seahorse XFe-96 proprietary software | Essen BioScience | N/A |
| R package scCorr | R project | Version 0.1 |
| **Other** | | |
| 100 $mm^2$ poly-D-lysine–coated plate | Corning | 356469 |
| non-tissue culture 6-well plates | Corning | 3736 |
| CD3/CD28 dynabeads | ThermoFisher | nc0985519 |
| Neon electroporation device | Life Technologies | MPK5000 |
| G-Rex 100 culture vessels | Wilson Wolf | P/N 80500 |
| ELISPOT plates | Cellular Technology Limited | hIFNgTNFa-1M/10 |
| Flow cytometer | Beckman Coulter | CytoFlex S orFortessa |
| Immunospot analyzer (for ELISPOT) | CTL Analyzers, LLC | CTL ImmunoSpot S6 Micro Analyzer |
| IncuCyte S3-Platform | Essen BioScience | |
| 10x Genomics Chromium Controller | 10x Genomics | GCG-SR-1 |
| LunaFL fluorescent cell counter | Logos Biosystems | L20001 |
| Chromium Single Cell 3′ GEM, Library & Gel Bead Kit v3 | 10x Genomics | PN-1000075 |
| Chromium Single Cell B Chip | 10x Genomics | PN-1000153 |
| NextSeq 500/550 platform | Illumina | SY-415-1001; SY-415-1002 |
| Xfe96 extracellular analyzer | Seahorse Bioscience | N/A |
| XF96 well plate | Seahorse Bioscience | 101085-004 |